ASN NEURO RESEARCH ARTICLE

ASN NEURO 2(5):art:e00046.doi:10.1042/AN20100022

Growth defects in the dorsal pallium after genetically targeted ablation of principal preplate neurons and neuroblasts: a morphometric analysis

Robin Fisher[1] and Yuan-Yun Xie[2]

Developmental and Molecular Neuroscience Group, Intellectual Development and Disabilities Research Center, Neuropsychiatric Institute, School of Medicine, The University of California at Los Angeles, Los Angeles, CA 90095, U.S.A.

Cite this article as: Fisher R and Xie Y-Y (2010) Growth defects in the dorsal pallium after genetically targeted ablation of principal preplate neurons and neuroblasts: a morphometric analysis. ASN NEURO 2(5):art:e00046.doi:10.1042/AN20100022

ABSTRACT

The present study delineates the large-scale, organic responses of growth in the dorsal pallium to targeted genetic ablations of the principal PP (preplate) neurons of the neocortex. Ganciclovir treatment during prenatal development [from E11 (embryonic age 11) to E13] of mice selectively killed cells with shared S-phase vulnerability and targeted expression of a GPT [golli promoter transgene; GPT linked to HSV-TK (herpes simplex virus-thymidine kinase), τ-eGFP and lacZ reporters] localized in PP neurons and their intermediate progenitor neuroblasts. The volume, area and thickness of the pallium were measured in an E12–P4 (postnatal age 4) longitudinal study with comparisons between ablated (HSV-TK$^{+/0}$) and control (HSV-TK$^{0/0}$) littermates. The extent of ablations was also systematically varied, and the effect on physical growth was assessed in an E18 cross-sectional study. The morphological evidence obtained in the present study supports the conclusion that genetically targeted ablations delay the settlement of the principal PP neurons of the dorsal pallium. This leads to progressive and substantial reductions of growth, despite compensatory responses that rapidly replace the ablated cells. These growth defects originate from inductive cellular interactions in the proliferative matrix of the ventricular zone of the pallium, but are amplified by subsequent morphogenic and trophic cellular interactions. The defects persist during the course of prenatal and postnatal development to demonstrate a constrained dose–response relationship with the extent of specific killing of GPT neurons. The defects propagate simultaneously in both the horizontal and vertical cytoarchitectural dimensions of the developing pallium, an outcome that produces a localized shortfall of volume in the telencephalic vesicles.

Key words: forebrain growth, morphogenesis, neocortex, pathogenesis, preplate, targeted ablation.

INTRODUCTION

The evolution of mammalian forebrain is dominated by the development of neocortex within the dorsal pallium (hereafter referred to as pallium). Early-generated PP (preplate) neurons are leading cells in this assembly, which links the phylogeny and ontogeny of neo-, juxtallo- and allo-cortex in the telencephalic marginal and mantle zones (Marin-Padilla, 1971, 1998). The principal PP neurons are believed to serve as a transient framework for the morphogenesis of neocortex via radial migration, laminar framing and guidance of afferent ingrowth (Luskin and Shatz, 1985; Ghosh and Shatz, 1993; Allendoerfer and Shatz, 1994; McConnell et al., 1994; Molnar and Blakemore, 1995; Ogawa et al., 1995; Valverde et al., 1995; Del Rio et al., 1997; Molnar et al., 1998; Super et al., 1998; Super and Uylings, 2001; Sarnat and Flores-Sarnat, 2002; Xie et al., 2002, 2009). They mould features of the vertical and the horizontal cytoarchitecture that are the structural foundations for the actions of mature neocortex (Jones, 1988).

[1] To whom correspondence should be addressed (email rfisher@mednet.ucla.edu).

[2] Present address: Centre for Molecular Medicine and Therapeutics, Department of Medical Genetics, University of British Columbia, Vancouver, BC, Canada, V5Z 4H4

Abbreviations: BrdU, bromodeoxyuridine; CP/D, cortical plate/distal division; CP/P, cortical plate/proximal division; df, degrees of freedom; E11, embryonic age 11; GPT, golli promoter transgene; HSV-TK, herpes simplex virus-thymidine kinase; IZ, intermediate zone; MBP, myelin basic protein; NA, numerical aperture; P_{α}, probability of type I error; P4, postnatal age 4; PP, preplate; SP, subplate; SVZ, subventricular zone; TUNEL, terminal deoxynucleotidyltransferase-mediated dUTP nick-end labelling; X-gal, 5-bromo-4-chloro-3-indolyl-β-D-galactoside; VZ, ventricular zone; VZ/SVZ, the combined VZ and SVZ.

© **2010 The Author(s)** This is an Open Access article distributed under the terms of the Creative Commons Attribution Non-Commercial Licence (http://creativecommons.org/licenses/by-nc/2.5/) which permits unrestricted non-commercial use, distribution and reproduction in any medium, provided the original work is properly cited.

Evidence based on the purported ablation of PP neurons plays an important role in this conceptual framework. However, these findings entail persistent issues with regard to the selectivity of ablations, the dearth of quantitative estimates of specific cell killing and the lack of systematic assessments of the impact of ablations on fundamental aspects of the phenotype such as forebrain growth. Our recent investigations address these issues by a powerful combination of molecular biological and neurochemical methods for the specific identification and reasonably selective ablation of the principal PP neurons in transgenic mice (Landry et al., 1998; Xie et al., 2002, 2009; Jacobs et al., 2007). The proximal GPT (golli promoter transgene) of the MBP (myelin basic protein) gene exhibits early and restricted expression in cerebral cortex, olfactory bulb and sensory ganglia. It can drive the expression of useful reporter genes, including HSV-TK (herpes simplex virus-thymidine kinase), for the structural identification of the principal PP neurons and their neuroblasts (hereafter referred to collectively as GPT cells). The GPT neurons match the morphological properties of the principal PP neurons because they proliferate from GPT-expressing intermediate progenitors confined to the dorsal pallial VZ (ventricular zone), undergo radial migration with a neurogenetic pattern of 'outside-in' settlement in the marginal and mantle zones, emit the earliest corticofugal pioneer axons and tend to show shorter periods of survival than cortical plate neurons.

When GPT drives the co-expression of HSV-TK, the prodrug ganciclovir can be converted into toxic nucleotide analogues that disrupt DNA synthesis in genetically targeted GPT progenitors. This initiates apoptosis in their daughter GPT cells (neurons and/or neuroblasts), which complete mitotic division after shared S-phase vulnerability (Moolten, 1986; Xie et al., 2009). Such treatments produce specific, transient and additive killing of as much as 90% of the normal complement of GPT cells. As shown in the initial qualitative survey of the ablation phenotype, the developing pallium presents a wide array of cell disarrangements that eventually result in retarded vertical growth and mild dyslamination, early defects that may be exacerbated by late-onset hydrocephalus (Xie et al., 2002). A subsequent quantitative analysis reveals the remarkable reorganization of pallial GPT neurons and neuroblasts in the ablation phenotype, which responds to their induced apoptosis by compensatory reconstitution of VZ progenitors, delayed settlement of GPT replacement neurons with a near-normal restoration of their total complement and failed emission of pioneer corticofugal axons (Xie et al., 2009). We now deploy a quantitative analysis of the large-scale regional organization of the pallium in the ablation phenotype, in order to test the hypothesis that the ablation of GPT cells impairs vertical, but not horizontal, growth within the pallium and its neocortical derivative. The developmental expansion of the pallium and its parts is compared in time series between littermate control and genetically targeted mice with equivalent exposures to ganciclovir during the early fetal period of generation of GPT cells. For the first time, the number of ganciclovir treatments and the ages at ganciclovir exposure are also varied systematically to determine whether the phenotypic growth defects of the ablation exhibit a dose–response relationship with the extent of specific GPT cell killing.

MATERIALS AND METHODS

Many of the methods used here were described fully in previous reports (Landry et al., 1998; Xie et al., 2002, 2009; Jacobs et al., 2007). New observations were obtained from 119 mice (74 HSV-TK$^{+/0}$ experimentals; 45 HSV-TK$^{0/0}$ controls) randomly selected from 24 timed pregnancies [day of mating=E0.5 (embryonic age 0.5; as defined by common use; technically, mice at ages greater than E7 are fetuses because the heart displays co-ordinated contraction), day of birth=P1 (postnatal age 1)]. Data from males and females were equivalent and pooled. Mice were housed in the UCLA School of Medicine vivarium, and procedures were conducted as per the NIH Guide for the Care and Use of Laboratory Animals.

Generation and ablation of transgenic mice

Establishment and histological identification of genotypes

Transgenic genotypes were produced using the proximal GPT for the MBP gene to drive expression of linked, non-native reporter transgenes for HSV-TK and lacZ galactosidase (lacZ; Landry et al., 1998; Xie et al., 2002, 2009). The GPT element inserted into all mice was a fragment containing 1.1 kb upstream of the golli transcription start site plus 0.2 kb downstream into the first exon of the MBP gene. Only one transgenic line was studied. Double transgenics were generated by crossing hemizygous HSV-TK and homozygous lacZ mice to produce HSV-TK$^{+/0}$/lacZ$^{+/+}$ (experimental) and HSV-TK$^{0/0}$/lacZ$^{+/+}$ (control, wild-type) mice.

Cross-validation of genotypes by PCR

The GPT/HSV-TK transgene was identified in founder breeders and all experimental mice by PCR using the MGTB sense primer 5′-CTGAGCTTCACGACCCCGGAACATAGT (within GPT) and the HSV-TK3P antisense primer 3′-GTCATGCTGCCCATA-AGGTATCGCG. The GPT/lacZ transgene was identified in all mice using the MGTB sense primer and the β-galactosidase antisense primer 3′-CTCATCCGCCACATATCCTGATCTTCC. For PCR amplification, a 25 µl reaction was assembled containing 200 ng of genomic DNA, 10 pmol of primer, 4 mM $MgCl_2$, 0.2 mM dNTPs, PCR buffer (Promega) and 1.25 units of Taq DNA polymerase (Invitrogen, Carlsbad, CA, U.S.A.). After denaturation, PCR products were analysed on 1% agarose TAE (Tris/acetate/EDTA) gel. As in previous reports (Landry et al., 1998; Xie et al., 2002; Jacobs et al., 2007), the HSV-TK

© 2010 The Author(s) This is an Open Access article distributed under the terms of the Creative Commons Attribution Non-Commercial Licence (http://creativecommons.org/licenses/by-nc/2.5/) which permits unrestricted non-commercial use, distribution and reproduction in any medium, provided the original work is properly cited.

reporter in experimental mice was 0.6 kb and the lacZ β-galactosidase reporter in all mice was 1.1 kb.

Ganciclovir treatments

Ganciclovir (Cytovene-IV™, Roche Laboratories, Nuffy, NJ, U.S.A.) was diluted to 0.25 mg/ml water vehicle. For large ablations in the main treatment group, pregnant dams received two intraperitoneal injections of ganciclovir (20 μg/g of body weight) on E11 and E12 (four injections at 10–12 h intervals; Xie et al., 2002, 2009). For smaller ablations to assess serial lesion effects, pregnant dams received ganciclovir treatments on the following schedules: three injections on E11–E12, two injections on E11, E12, E13, E14, E15 or E17, one injection on E11, one injection on E12 and one injection on E11 (genotypes, treatment ages and ganciclovir treatment schedules shown in Figure 9). Treatment age groups were selected due to positive expression of HSV-TK in pallial VZ progenitors of unablated experimental mice on E11–E13 (Xie et al., 2009). Experimental mice that received vehicle instead of ganciclovir on E11–E12, or ganciclovir on E14–E17, had no damage. All mice were alive at delivery as shown by spontaneous movement.

Histological preparations

Tissue processing

Pregnant dams were anaesthetized with halothane and terminated by cervical dislocation to obtain fetal tissue on E12–16 and E18. Fetuses were delivered, brains dissected and tissues immersed in 0.9% (w/v) NaCl and 4% (w/v) paraformaldehyde in 0.1 M PBS fixative. Postpartum mice were anaesthetized with halothane and perfused transcardially with fixative to obtain tissue on P1 and P4. Tissues were immersion-fixed for 1 h at 4 °C, cryoprotected for 24 h in 30% (w/v) sucrose, frozen in OCT™, sectioned serially at 20 μm thickness in the coronal plane and mounted on subbed glass slides. The section interval was 400 μm along the rostrocaudal axis of the forebrain.

Mice were terminated mainly on two age schedules designed to establish (i) a longitudinal time series for assessment of the development of the phenotypic features of the ablations and (ii) a late cross-sectional index age for assessment of persistent ablation defects. For (i), mice from one small treatment group (two ganciclovir injections on E11) were terminated on E12 and mice from the main treatment group (four ganciclovir injections on E11 and E12) were terminated on E13–16, E18, P1 and P4 for the time series from E12 to P4. For (ii), mice from all treatment groups were terminated at E18 as the index age in order to obtain measurements after the substantial accumulation of growth defects, but before the later advent of potentially complicating processes of myelination in all mice and hydrocephalus in mice with severe ablations.

lacZ β-galactosidase histochemistry

Mounted sections were treated in 0.01% sodium deoxycholate, 0.02% Nonidet P40, 2 mM $MgCl_2$ and 0.1 M $NaHPO_4$ (pH 7.3) for 10 min at room temperature (25 °C) and then incubated in X-gal (5-bromo-4-chloro-3-indolyl-β-D-galactoside) labelling solution [2 mM $MgCl_2$, 5 mM $K_3Fe(CN)_6$, 5 mM $K_4Fe(CN)_6$ plus 0.1 M $NaHPO_4$, pH 7.3, 0.01% sodium deoxycholate, 0.02% Nonidet P40 and 8 mg/ml X-gal] for 6–16 h at 37 °C followed by a PBS stop-bath. Method specificity of labelling of GPT neurons was confirmed by omission of X-gal treatment in 'control' sections from each case. Labelled sections were used for co-localization experiments and counterstained in some cases with Neutral Red (Figure 5; ten cases), which optimized photomacroscopy, and/or Harris haematoxylin (regressive method; all cases), for improved high-contrast recognition of degenerating cells, mitotic profiles and pallial laminae.

Other background materials

Additional serial sections were obtained from many of the cases and used for a variety of modern multiple labelling studies included in our previous report (cf. Xie et al., 2009, for details of specimen production and measurement). LacZ-labelled cells in control and ablated mice were compared for determining the impact of ganciclovir treatment on the densities of GPT neurons, while pyknosis and TUNEL (terminal deoxynucleotidyltransferase-mediated dUTP nick-end labelling) labelled cells were compared for assessing the impact of ganciclovir treatment on the densities of apoptotic cells. Sections obtained from other control and ablated mice of comparable ages were also used for double-labelling studies to cross-validate the developmental patterns of expression of lacZ and HSV-TK reporters in GPT neurons. Finally, sections from other control and ablated mice were used for double-labelling studies to determine the ages when GPT neurons and neuroblasts were generated, as shown by incorporation of BrdU (bromodeoxyuridine). Data from these studies were used to quantitatively estimate by ablation group (but not by case within each ablation group) the extent of specific cell killing during the initial phase of the ablation, which divided ablation groups on the basis of ratio instead of nominal scale values for parametric statistical analyses.

Morphological analysis

Histological differences were assessed by comparisons between and within genotype, treatment and age groups. Observations were obtained by light microscopy with bright-field transmission illumination (Zeiss Ultraphot IIIB and Leica DMRXA microscopes). Data were recorded by analogue film and digital photography, as well as by *camera lucida* mapping.

Trends observed by qualitative methods were pursued by quantitative measurements, mainly volumetric, horizontal areal and vertical linear indices of the pallium and its parts, to assess the statistical reliability of differences between groups. Measurements were obtained bilaterally from each case in each group (115 total measured cases; 72 ablated mice; 43

© 2010 The Author(s) This is an Open Access article distributed under the terms of the Creative Commons Attribution Non-Commercial Licence (http://creativecommons.org/licenses/by-nc/2.5/) which permits unrestricted non-commercial use, distribution and reproduction in any medium, provided the original work is properly cited.

control mice). Developmental patterns of co-extensive pallium and neocortex were bilaterally symmetric in all groups, so measurements were averaged across hemispheres in each case. The pallium had a lateral-to-medial horizontal neurogenetic gradient reflected in the vertical extent and density of neocortical GPT neurons, so sampling sites for vertical linear indices were selected from its flat-mapped centre where measurements approximated averages from lateral and medial limits. Lateral and medial boundaries of neocortex within pallium were denoted by distinct breaks in densities of labelled GPT neurons near the cingulum and rhinal sulcus, while ventricular and pial surfaces were proximal and distal boundaries for volumetric and horizontal areal measurements (Figures 3 and 5). The laminar distribution of haematoxylin-stained cell bodies between ventricular and pial surfaces denoted the boundaries of each component for vertical linear measurements. Some, but not all, ablated mice had pallial scars, which obliterated all laminar boundaries. These scars contained few if any GPT or non-GPT neurons, so they were measured as a separate part of total values obtained for volumetric and horizontal areal indices. Sampling sites selected for vertical linear measurements were always in unscarred pallium to assure homologous locations, well-lateral to scars, between groups.

Design considerations and scales of measurements

The logical status of variables and the nature of their measurements merited close consideration because of the central role of statistical analyses in the present study. Dependent variables based on volume, area and thickness were ratio scale measurements used to estimate the growth of pallium. Ablation first served as a dependent variable to estimate the specific killing of GPT neurons during and shortly after ganciclovir treatment. For convenience, independent variables are denoted in italics in the remainder of this paper. *ablation* was used subsequently as an intervening, independent variable to probe the relationship between the magnitudes of specific killing of GPT neurons and pallial growth. Depending on the requirements of statistical analyses, *ablation* could be characterized by ratio or ordinal scale values. *Age* was an independent variable tested for the influence on the generation of ablations and pallial growth. It was characterized by ratio scale measurements.

Volumetric measurements

The series of sections from each case was drawn by *camera lucida* at a total projected magnification of $\times 65$ [E12–E14 groups; $\times 4$ zoom objective, NA (numerical aperature)$=0.09$] or $\times 32.5$ (E15–P4 groups; $\times 2$ zoom objective, NA$=0.05$; Figure 3). The boundaries of the pallium with neocortex on each tissue section, including scars when present, were marked, based on microscopic observations of lacZ and haematoxylin-stained cells, and then measured bilaterally by planimetry (Teledyne Post planimeter; Figure 5, lines A-A′-B′-B). Areal values were expanded by section interval to estimate total volume, scar volume (when present) and unscarred volume of pallium, with a shrinkage correction of 10% in each of the three measured dimensions. Values were averaged across cerebral hemispheres for each case and then averaged across cases for each genotype, treatment and termination age group. Grouped data for each time series were compared statistically, mainly by two-way ANOVAs and pairwise Student's *t* tests with fixed values of P_α (probability of type I error) <0.01 and <0.05 respectively [one-tailed tests; the latter demonstrated graphically by non-overlapping means $\pm$ S.E.M. ($\overline{X} \pm$ S.E.M.)] as the criteria of reliable differences between groups (Ferguson, 1971; UCLA Statistics Online Computational Resource). The volumes of VZ/SVZ [the combined VZ and SVZ (subventricular zone)], which incorporated the pallial proliferative matrices, were measured and compared in the same fashion.

Pallial volume was further divided in each case in order to uncover regional differences in growth. For lateral versus medial comparisons, the boundary between the lateral and medial pallium was the dorsomedial peak of neocortex. This landmark had a relatively fixed position throughout development, and was associated with scars, when present, in ablated mice. For anterior versus posterior comparisons, the boundary between the anterior and the posterior pallium was a midsection in each series. This boundary varied with age, had no surface landmark and was often associated with the midpoint of scars in ablated mice. The time series of grouped data were compared statistically by three-way ANOVAs and pairwise Student's *t* tests with fixed values of $P_\alpha<0.01$ and $P_\alpha<0.05$ respectively (one-tailed tests) as the criteria of reliable differences between groups (Ferguson, 1971) (StatPlus, 2008; http://www.analystsoft.com). For brevity, only the decisions based on these analyses, with ranges of statistical values and their appropriate degrees of freedom (df), are detailed below.

Horizontal areal measurements

The length of the pial boundary of the pallium associated with neocortex was measured on each *camera lucida* drawing from the series of sections obtained from each case (Alvin Plan Measure; Figure 5, lines A-A′). Linear values were expanded by section interval to estimate pallial total area, scar area (when present) and unscarred area, with a shrinkage correction of 10% in each of the two measured dimensions. Values were averaged across cerebral hemispheres for each case and then averaged across cases for each genotype, treatment and termination age group. Grouped data for each time series were compared statistically, as detailed above. VZ/SVZ areas were measured and compared in the same fashion using the length of the ventricular boundary of the pallium underlying neocortex (Figure 5, lines B-B′).

Vertical thickness measurements

The thicknesses of the pallium and its laminar components were measured by direct microscopic observations of a

© 2010 The Author(s) This is an Open Access article distributed under the terms of the Creative Commons Attribution Non-Commercial Licence (http://creativecommons.org/licenses/by-nc/2.5/) which permits unrestricted non-commercial use, distribution and reproduction in any medium, provided the original work is properly cited.

sampling line placed between, and orthogonal to, the pial and ventricular surfaces ($\times$391 total magnification; $\times$25 objective, NA=0.65) of a midsection in the series obtained from each case (Figure 5, lines C-C′). Linear values were expanded by a shrinkage correction of 10% in the measured dimension. Values were averaged across cerebral hemispheres for each case and then averaged across cases for each genotype, treatment and termination age group. Grouped data for each time series were compared statistically, as detailed above.

Cell densities were also measured in the developing laminar components of the pallium. Intercepts of cells with nuclear profiles were detected by light microscopy ($\times$40 objective, NA=0.90, $\times$1000 total magnification). For each laminar component, cell intercepts were counted along a measurement line (143 μm) placed horizontally to the vertical sampling line in a midsection from each case. Values were expanded by a shrinkage correction of 10% in the measured dimension, and an Abercrombie correction of 0.8 consistent with a 20 μm section thickness and an average nuclear diameter of 5 μm (Guillery, 2002). Values were extrapolated to yield cell density per mm of tissue measured, averaged across cerebral hemispheres for each case, and then averaged across cases for each genotype, treatment and age group. Grouped data for each time series were compared statistically, as detailed above.

RESULTS

Characterization of ablations

GPT cells in the dorsal pallium proved to be the exclusive targets for specific killing. Neocortical GPT neurons were normally generated by neuroblasts (intermediate progenitor cells that also expressed GPT) with restricted locations in the pallial VZ on E11–E13 (40% on E11, 50% on E12 and 10% on E13 for total GPT neuron complement; Xie et al., 2009). The initial ablation phenotype, as defined by transient excesses of apoptotic GPT cells (Van Cruchten and Van den Broek, 2002; D'Herde et al., 2003), was observed only in experimental mice with ganciclovir treatments on E11–E13, in accord with a genetically targeted attack on GPT intermediate progenitors. All mice that met these three necessary and sufficient conditions had an ablation, while all mice that failed to meet even one condition had no ablation. Thus the occurrence of the ablation phenotype was reliably determined by three independent variables and/or their interactions: *genotype*, *ganciclovir treatment* and *age at treatment*.

Longitudinal comparisons of control and ablated mice showed that the full expression of the pallial ablation phenotype was generated in three sequential phases of apoptosis and accumulation of GPT neurons (Xie et al., 2009). The first phase of massive early-onset apoptosis in the ventricular and mantle zones occurred during and shortly after ganciclovir treatments on E11–E13, coincident with suppressed accumulation of GPT neurons in the mantle zone. A second phase of middle-onset apoptosis restored normal background levels of cell death on E14–E16, coincident with reconstitution of the VZ and replacement of GPT neurons in the mantle zone. The third phase of late-onset apoptosis resumed moderately elevated levels of cell death, coincident with slow dissolution of GPT neurons in the mantle zone after E16. Growth defects, which were inherent to the full ablation phenotype, began in the first phase and progressed thereafter. They involved both GPT and non-GPT cells.

The effective combinations of *genotype*, *ganciclovir treatment* and *age at treatment* had a dose–response relationship with the initial, transient reductions of pallial GPT neurons, concomitant with their specific killing, in ablated mice (Xie et al., 2009). Treatments at 12 h intervals produced additive serial ablations. Each treatment reduced the accumulation of viable GPT neurons in the subsequent 12 h period to 10% of GPT neurons normally generated by the cohort of GPT neuroblasts available at the beginning of the period, as shown by BrdU incorporation (i.e. at this stage of the ablation phenotype, the principal constraint on the extent of specific killing was the number of vulnerable target cells present at the age of ganciclovir exposure). As shown by pyknosis and TUNEL, the simultaneous accumulation of killed cells doubled the proportion of 'missing' GPT cells ($2 \times 90\% = 180\%$). These observations showed that the genetically targeted ablation was a selective attack on GPT intermediate progenitors, which gave rise by asymmetric cell division to daughter GPT neuroblasts and GPT neurons (Smart, 1973; Chenn and McConnell, 1995; Pontious et al., 2008). As derivative values calculated from these observations, ablated mice with two E11 treatments and E12 termination had a predicted 90% reduction of GPT neurons normally present on E12. Ablated mice with four E11–E12 treatments and E13 termination had a predicted 90% reduction of GPT neurons normally present on E13. Ablated mice with four E11–E12 treatments and E14 termination had a predicted 81% ($90\% \times 90\%$) reduction of the original complement of GPT neurons normally present on E14 (after proliferative exhaustion of normal GPT neuroblasts on E13). For the longitudinal study, data were pooled and ablated mice at all termination ages were considered to have minimum permanent 81% reductions of original (but not replacement or permanent total) complements of GPT neurons. For the cross-sectional study, permanent reductions of original complements of GPT neurons in ablation groups were: 81% (four E11–E12 treatments), 70% (three E11–E12 treatments), 45% (two E12 treatments), 41% (one E11 treatment and one E12 treatment), 36% (two E11 treatments), 18% (one E11 treatment) and 9% (two E13 treatments). The derivative predictions were cross-validated by direct observations from four key groups of mice. Average densities of GPT neurons were expanded by volumes of unscarred neocortex and then compared between control and ablated mice terminated at ages during and shortly after ganciclovir treatment. After two ganciclovir treatments on E11, ablated mice terminated on

© 2010 The Author(s) This is an Open Access article distributed under the terms of the Creative Commons Attribution Non-Commercial Licence (http://creativecommons.org/licenses/by-nc/2.5/) which permits unrestricted non-commercial use, distribution and reproduction in any medium, provided the original work is properly cited.

E12 had an 84% reduction in the complement of GPT neurons normally present on E12. After four treatments on E11–E12, ablated mice terminated on E13 had an 83% reduction in the complement of GPT neurons normally present on E13. After four treatments on E11–E12, ablated mice terminated on E14 had a 56% reduction due to replacement of GPT neurons killed on E11, absence of GPT neurons killed on E12 (45%) and delayed settlement of GPT neurons normally generated on E13 (10%). After two treatments on E12, ablated mice terminated on E14 had a 54% reduction due to unablated GPT neurons generated on E11, absence of GPT neurons killed on E12 (45%) and delayed settlement of GPT neurons normally generated on E13 (10%). Minor differences between predicted and observed neuron reductions at 24 h after the end of ganciclovir treatments were due to misclassification of cells in early stages of apoptosis. By E14, most of the specifically killed apoptotic cells were cleared from the pallium.

Longitudinal study of growth reduction in the dorsal pallium of ablated mice

The most important results of the present paper are shown in Figures 1(A)–1(C), where pallial volume, area (at the pial surface) and thickness were plotted against age groups and compared between ablation groups in the longitudinal study. Two-way ANOVAs demonstrated the overall statistical significance of both *ablation* [**F**=69.1–288.2, degrees of freedom (df)=1,64; $P_\alpha<0.01$] and *age* (**F**=61.9–305.8; df=7,64; $P_\alpha<0.01$) main effects, and the *ablation* × *age* interaction (**F**=32.2–110.5; df=7,64; $P_\alpha<0.01$), on volume, area and thickness between E12 and P4. Growth of all dependent variables occurred as an additive function of age in control and ablated mice, regardless of the source of volume and area measurements in total (scarred plus unscarred) or unscarred pallium (Figures 1A and 1B). Within the additive function of age in ablated mice, pallial growth was also progressively reduced regardless of scar inclusion. Graphic comparisons at each age level showed statistically reliable differences between control and ablated mice for the cumulative growth of all three dependent variables on and after E13 (Figures 1A–1C; Student's *t* tests; df=6–8; $P_\alpha<0.05$). No reliable differences were obtained between cerebral hemispheres on any of these measurements.

The graphs also demonstrate that statistical requirements of homogeneity of variance and linearity were fulfilled for all dependent variables in the tested study period. Thus ANOVA coefficients of determination for volume (control versus ablated total pallium $\overline{R}^2=0.82$; control versus ablated unscarred pallium $\overline{R}^2=0.79$) represented the total proportions of variance due to *ablation* and *age* main effects, and the *ablation* × *age* interaction. Slightly greater $\overline{R}^2$ values were obtained for surface area (control versus ablated total pallium $\overline{R}^2=0.89$; control versus ablated unscarred pallium $\overline{R}^2=0.85$) and thickness (control versus ablated pallium $\overline{R}^2=0.91$). These robust values revealed the sufficiency of a linear model with two main effects to account for the differences observed between the groups.

The trends for all three dependent variables had early deflections ('hinge regions') that reflected stalled growth, but not tissue loss, in the ablated pallium between E11 and E13, coincident with the first phase of apoptosis associated with the specific killing of GPT neurons (Figure 1). Late deflections reflected a second period of stalled growth of volume and area in the ablated pallium between E15 and E16, near the close of the second phase of suppressed apoptosis associated with the restoration of GPT neurons. The relatively small scale of these deflections did not hamper linear regression of dependent variables with age, which generated predicted E11 'pretreatment' values and slopes, a useful single-value indicator of growth rate.

Quantitative volume defects

Pallial volume in control mice increased from 0.46 ± 0.10 mm^3 ($\overline{X}\pm$S.E.M.) to 13.32 ± 0.62 mm^3 between E12 and P4, a measured cumulative growth of 2796% (calculated from P4–E12/E12 values; Figure 1A). Volume was reliably correlated with age (Pearson product–moment correlation coefficient **r**=0.95; df=36; $P_\alpha<0.05$) with a growth rate (identical with the slope of the linear regression equation) of 1.10 mm^3/day. The predicted E11 volume (0.36 mm^3) yielded a cumulative growth of 3600% (P4–E11/E11 values).

Pallial total volume in ablated mice increased from 0.36 ± 0.04 to 7.04 ± 0.86 mm^3 between E12 and P4, a measured cumulative growth of 1856%. The total volume was reliably correlated with age (**r**=0.89; df=38; $P_\alpha<0.05$) with a growth rate of 0.52 mm^3/day, less than half of the control value. The predicted E11 total volume (0.36 mm^3, the predicted E11 control value) yielded a cumulative growth of 1856% in ablated mice. At P4, the predicted total volume in ablated mice was 52% of the control value, similar to an observed reduction to 53% (i.e. a 47% growth shortfall).

Pallial unscarred volume in ablated mice increased from 0.36 ± 0.04 to 5.86 ± 0.84 mm^3 between E12 and P4, a measured cumulative growth of 1528%. Unscarred volume was reliably correlated with age (**r**=0.87; df=38; $P_\alpha<0.05$) with a growth rate of 0.44 mm^3/day, less than half of the control value. The predicted E11 unscarred volume (0.36 mm^3) yielded a cumulative growth of 1528% in ablated mice. At P4, the predicted unscarred volume in ablated mice was 42% of the control value, similar to an observed reduction to 44% (a 56% growth shortfall).

Scars were observed in all ablated, and no control, mice in the longitudinal study on and after E13. Pallial scar volume increased from 0.06 ± 0.01 to 1.18 ± 0.09 mm^3 between E13 and P4, a cumulative growth of 1867%. The scar growth rate was 0.08 mm^3/day, less than 20% of the growth rate in adjacent, unscarred pallium. Scars were less than 10% of pallial total volume until P1, with rapid expansion to 17% on P4.

© 2010 The Author(s) This is an Open Access article distributed under the terms of the Creative Commons Attribution Non-Commercial Licence (http://creativecommons.org/licenses/by-nc/2.5/) which permits unrestricted non-commercial use, distribution and reproduction in any medium, provided the original work is properly cited.

Quantitative area defects

Pallial area in control mice increased from 3.5 ± 0.4 to 24.6 ± 1.4 mm^2 between E12 and P4, a measured cumulative growth of 603% (Figure 1B). Area was reliably correlated with age (**r**=0.94; df=36; P_α<0.05) with a growth rate of 1.6 mm^2/day. The predicted E11 area (2.8 mm^2) yielded a cumulative growth of 779%.

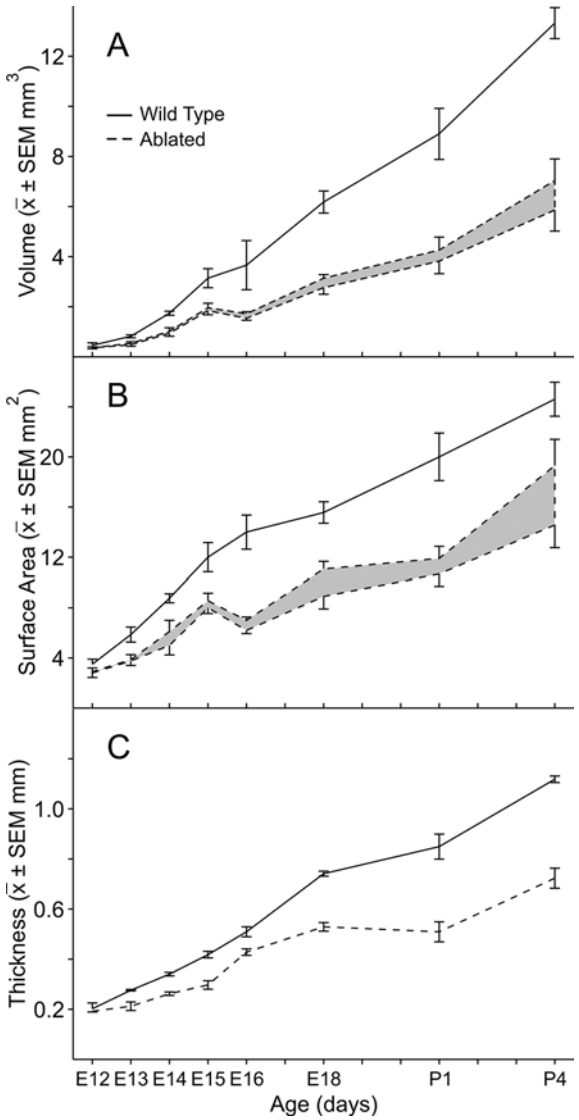

Figure 1 Mean volume (A), surface area (at pial interface) (B) and thickness (C) ($\bar{X}$ ± S.E.M.) of the dorsal pallium in wild-type (control) and ablated mice plotted as a function of age from E12 to P4

These results represent the longitudinal time-series study where four ganciclovir treatments were administered on E11–E12. For ablated mice in (**A**) and (**B**), the upper trends represent $\bar{X}$+S.E.M. total (scarred plus unscarred) volumes and surface areas, whereas the lower trends represent $\bar{X}$−S.E.M. unscarred volumes and surface areas. Shaded areas between upper and lower trends for ablated mice represent scarred dorsal pallium. Two-way ANOVAs demonstrate the statistical reliability of *ablation* and *age* main effects, and the *ablation* × *age* interaction, for overall comparisons between control and ablated mice during this developmental period on each measure of volume, surface area and thickness (P_α<0.01, one-tailed tests). Student's *t* tests and non-overlapped $\bar{X}$+S.E.M. demonstrate the statistical reliability of differences between pairwise contrasts of data from individual age groups (P_α<0.05, one-tailed tests).

Pallial total area in ablated mice increased from 2.9 ± 0.3 to 19.3 ± 2.1 mm^2 between E12 and P4, a measured cumulative growth of 566%. Total area was reliably correlated with age (**r**=0.92; df=38; P_α<0.05) with a growth rate of 1.2 mm^2/day, 75% of the control value. The predicted E11 total area (2.8 mm^2) yielded a cumulative growth of 589% in ablated mice. At P4, the predicted total area in ablated mice was 76% of the control value, similar to an observed reduction to 78% (a 22% growth shortfall).

Pallial unscarred area in ablated mice increased from 2.8 ± 0.3 to 14.6 ± 1.8 mm^2 between E12 and P4, a measured cumulative growth of 421%. Unscarred area was reliably correlated with age (**r**=0.89; df=38; P_α<0.05) with a growth rate of 0.9 mm^2/day, 56% of the control value. The predicted E11 unscarred area (2.8 mm^2) yielded a cumulative growth of 421% in ablated mice. At P4, the predicted unscarred area in ablated mice was 54% of the control value, which approximated an observed reduction to 59% (a 41% growth shortfall).

Pallial scar area increased from 0.1 ± 0.01 to 4.7 ± 0.5 mm^2 between E13 and P4, an overall measured growth of 4600%. The scar area growth rate of 0.34 mm^2/day was 38% of the growth rate in adjacent, unscarred pallium. Scars were less than 20% of the pallial total area in ablated mice until P1, followed by expansion to 25% on P4.

Quantitative thickness defects

Pallial thickness in control mice increased from 0.20 ± 0.02 to 1.12 ± 0.01 mm between E12 and P4, a measured cumulative growth of 460% (Figure 1C). Thickness was reliably correlated with age (**r**=0.98; df=36; P_α<0.05) with a growth rate of 0.08 mm/day. The predicted E11 thickness (0.19 mm) yielded a cumulative growth of 489%.

Pallial thickness in ablated mice increased from 0.19 ± 0.01 to 0.72 ± 0.04 mm between E12–P4, a measured cumulative growth of 279%. Thickness was reliably correlated with age (**r**=0.94; df=38; P_α<0.05) with a growth rate of 0.04 mm/day, 50% of the control value. The predicted E11 thickness (0.19 mm) yielded a cumulative growth of 279% in ablated mice. At P4, the predicted thickness in ablated mice was 57% of the control value, identical with an observed reduction to 57% (a 43% growth shortfall).

The thicknesses of scarred and unscarred pallium in ablated mice were comparable from E11 to P1. Scars thinned to approx. 75% of values in adjacent, unscarred pallium between P1 and P4.

Interrelationships of volume, area and thickness

The dependent variables of pallial volume, area and thickness were measured by different methods, but all three expanded on the same time course in control and ablated mice, and demonstrated comparable levels of growth reductions for

© 2010 The Author(s) This is an Open Access article distributed under the terms of the Creative Commons Attribution Non-Commercial Licence (http://creativecommons.org/licenses/by-nc/2.5/) which permits unrestricted non-commercial use, distribution and reproduction in any medium, provided the original work is properly cited.

unscarred pallium in ablated mice. Reliable intercorrelations were observed between the dependent variables, which indicated their high degree of internal validity between E12 and P4. For pallium in control mice, the values for **r**=0.97 (volume versus area), 0.95 (volume versus thickness) and 0.95 (area versus thickness) (df=36; $P_\alpha<0.05$). For total pallium in ablated mice, respective values for **r**=0.98, 0.85 and 0.88 (df=38; $P_\alpha<0.05$). For unscarred pallium in ablated mice, respective values for **r**=0.98, 0.82 and 0.83 (df=38; $P_\alpha<0.05$). Under the present conditions, each dependent variable could have served as a useful surrogate for the other two dependent variables. Within spatial constraints (i.e. pallium developed as a curved, truncated, conical hemisection, not a flat, semicircular plate), volume was an approximate product of surface area and thickness. In ablated mice, surface area was a better predictor than thickness of total and unscarred volume, indicative of a slight dissociation of dependent variables.

Interrelationships of horizontal regionalization and volume

The pallium of rodents has a lateral-to-medial neurogenetic gradient of development (Bayer and Altman, 1991). Gradient influence on the growth of unscarred pallium in ablated mice was tested by addition of a third independent variable, *site* (horizontal regionalization in medial versus lateral divisions) to the ANOVA linear model, which had main effects of *site* (df=1124), *age* (df=7124) and *ablation* (df=1124) as well as interactions of *site* × *age* (df=7,124), *site* × *ablation* (df=1,124), *age* × *ablation* (df=7,124) and *site* × *age* × *ablation* (df=7,124). Results are shown in Figures 2(A) and 2-(B). Three-way ANOVA revealed the overall statistical significance of all main effects and interactions on pallial unscarred volume between E12 and P4 (**F**=3.9–524.7; $P_\alpha<0.01$), with preferential reduction of growth in the medial pallium of older ablated mice (Figures 3 and 4).

The graphs demonstrated that statistical requirements of homogeneity of variance and linearity were approximated for the dependent variable and tested study period. The adjusted, unbiased $\overline{R}^2$ coefficient of determination for pallial unscarred volume in the three-way ANOVA was 0.94, which represented the total proportion of variance due to the full complement of main effects and interactions. Relative to the $\overline{R}^2$ for unscarred volume in the two-variable linear model (0.79), the three-variable linear model provided a modest gain in sufficiency at the cost of inordinate complexity. For the most part, the simpler two-variable linear model was adequate for present needs. However, it was interesting to note that crucial *site* × *ablation* and *site* × *age* × *ablation* interactions of the three-way ANOVA were not statistically reliable when used to test anterior–posterior neurogenetic gradients (Figures 2C and 2D; $P_\alpha>0.01$), negative results consistent with a suspected absence of such gradients in the pallium (Bayer and Altman, 1991).

Physical recognition of growth defects

The occurrence of pallial growth defects in ablated mice was readily detected in the physical evidence obtained from tissue sections employed for measurements. Figure 3 is a composite of serial sections reconstructed from control (wild-type) and ablated mice from E12–P4, where pallium was designated in each section. It is notoriously difficult for human observers to assess numerical magnitudes of volume differences based solely on visual inspection, but pallial volume in each series for both groups clearly increased with age. Furthermore, pallial volume in each series from a control mouse was greater than the volume from an ablated mouse of the same age. Finally, pallial surface area and thickness varied in association with pallial total volume throughout the composite, so representative observations were congruent with quantitative measurements. The reconstructions also indicated that same-age control and ablated mice could not be reliably distinguished by simple visual comparisons of volumes occupied by telencephalic hemispheres. Ablated mice showed no gross microcephaly or microtelencephaly, even though relative volumes of lateral ventricles increased after E18 as a sign of progressive hydrocephalus.

Figure 4 is a composite of average surface area measurements reconstructed from control and ablated mice from E12–P4. Mapped measurements from serial sections were centred and aligned on the dorsomedial peaks of the pallium. This protocol did not accurately reflect the posterior divergence of supratentorial portions of telencephalic vesicles from the midline (Valverde, 1998), but it better represented the narrow alignment of scars, when present, between medial and lateral pallial divisions. Pallial superficial (pial) and deep (ventricular) areas were aligned and superimposed, with scars designated in ablated mice. In flat maps, pallial areas increased with age in both groups, although the extent of growth was reduced in the ablated group. Once more, graphic results agreed with quantitative measurements. They clearly showed the spatial association between scars and the central region of the pallial VZ in ablated mice, with gross expansion of the VZ after E18, and scars after P1.

Serial section and flat map reconstructions allowed judicious selection of representative sections for tests of additional, perhaps more efficient, measurements. Selection based on a criterion of maximum section size within each serial reconstruction supported the measurement of dependent variables for height (dorsal–ventral axis) and width (medial–lateral axis) of telencephalic vesicles, while the number of sections in each serial reconstruction allowed the measurement of a dependent variable for length (anterior–posterior axis) as the third spatial dimension (results not shown). Two-way ANOVAs demonstrated the overall statistical significance of *ablation* and *age* main effects, and the *ablation* × *age* interaction, on height, width and length of telencephalic vesicles between E12 and P4 (**F**=7.6–809.7; df as in previous two-way ANOVAs; $P_\alpha<0.01$). Growth was a reliable function of age in both groups, but less growth occurred in ablated mice. However, side-by-side examinations

© 2010 The Author(s) This is an Open Access article distributed under the terms of the Creative Commons Attribution Non-Commercial Licence (http://creativecommons.org/licenses/by-nc/2.5/) which permits unrestricted non-commercial use, distribution and reproduction in any medium, provided the original work is properly cited.

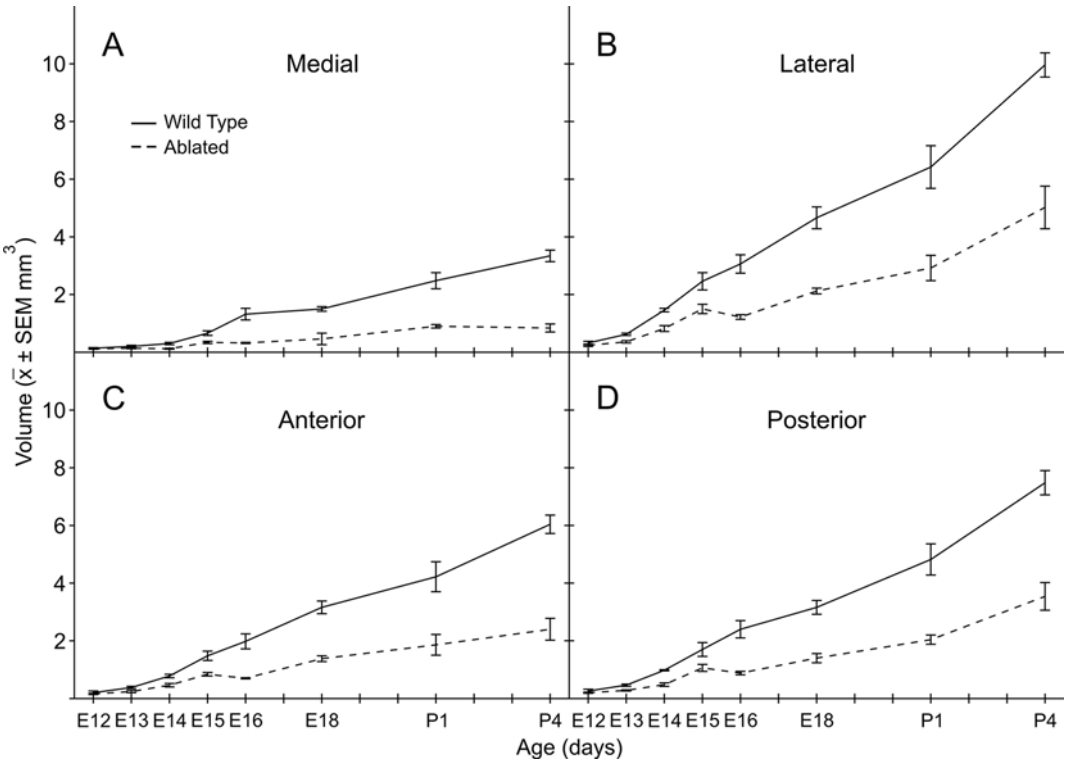

Figure 2 **Mean volumes of unscarred dorsal pallium ($\overline{X} \pm$S.E.M.) of the dorsal pallium in wild-type (control) and ablated mice plotted as a function of site and age from E12 to P4**

These results represent the longitudinal time-series study where four ganciclovir treatments were administered on E11–E12. Patterns of development for unscarred dorsal pallium are compared between the medial (**A**) versus the lateral (**B**) dorsal pallium, divided at the anatomical landmark of its dorsomedial peak. Three-way ANOVA demonstrates the statistical reliability of *site*, *age* and *ablation* main effects, *site* × *age*, *site* × *ablation* and *age* × *ablation* interactions and the *site* × *age* × *ablation* interaction (P_α<0.01, one-tailed tests) for this comparison. Patterns of development for unscarred dorsal pallium are also compared between the anterior (C) versus the posterior (D) dorsal pallium, divided at the axial midsection of the telencephalic vesicle. Three-way ANOVA fails to demonstrate the statistical reliability of a *site* main effect or any of its interactions for this comparison (P_α>0.01, one-tailed tests). Student's *t* tests and non-overlapped $\overline{X}$+S.E.M. demonstrate the statistical reliability of differences between pairwise contrasts of data from individual age groups (P_α<0.05, one-tailed tests).

of superficial aspects of telencephalic vesicles, in whole brains or serial section reconstructions, presented a paradox because there were no apparent differences between same-age control and ablated mice. The relatively small average reductions in ablated mice (5–10%) accounted for the discrepancy.

Selection based on a criterion of minimum pallial thickness had photomicrographic results shown in Figures 5(A) and 5(B) for E14 mice. Pallial areas outlined in control mice were greater than areas outlined in same-age ablated mice. Pallial lengths at the pial surfaces in control mice were greater than lengths in ablated mice. Pallial thicknesses in control mice were greater than thicknesses in ablated mice. Taken together, these macroscopic results corresponded to the results of quantitative measurements. But these specimens also uncovered the distribution and density of GPT neurons within the pallium, shown here during their second phase of replacement and apparent excess density when viewed next to same-age control tissue. This pallial pattern of replacement GPT neurons presented a second paradox because, compared with E14 control mice, the average measured density of GPT neurons/mm^3 of pallium was only 17% greater, and the total complement of pallial GPT neurons was 57% less, in E14 ablated mice. Large-scale growth defects and dyslamination accounted for the discrepancies.

Laminar distribution of vertical growth defects

The vertical organizations of pallial laminae were equivalent in control and ablated mice. Some laminae were developmentally transient, and their compositions were transformed with age. VZ/SVZ was considered to be a unitary neuroepithelial matrix, where thickness ultimately decreased with age due to proliferative exhaustion. By E18, a periventricular ependymal cell layer (post-mitotic) was separated from a paraventricular SVZ (mitotic) in control and ablated mice. The IZ (intermediate zone) contained cells migrating towards distal neocortical destinations throughout the E12–P4 study period. In older control mice, it also contained commissural (corpus callosum) and decussated (particularly subcallosal corticostriatal) fibres, which did not form in the severely ablated mice used for the

© 2010 The Author(s) This is an Open Access article distributed under the terms of the Creative Commons Attribution Non-Commercial Licence (http://creativecommons.org/licenses/by-nc/2.5/) which permits unrestricted non-commercial use, distribution and reproduction in any medium, provided the original work is properly cited.

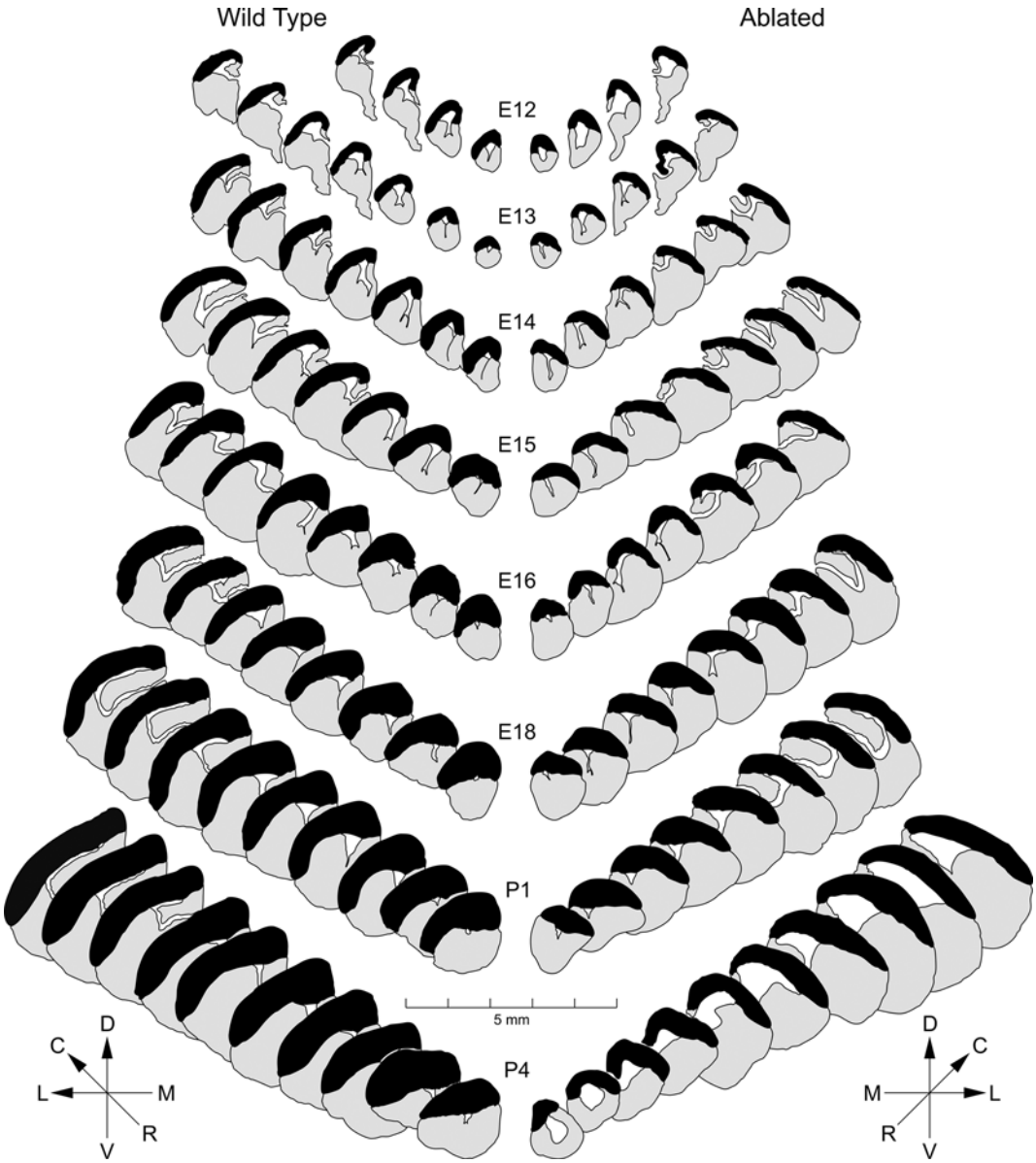

Figure 3 ***Camera lucida*** **maps of serial section reconstructions in the coronal plane of telencephalic vesicles in wild-type (control; left) and ablated (right) mice from E12 (top) to P4 (bottom)**

These results represent the longitudinal time-series study where four ganciclovir treatments were administered on E11–E12. Each reconstruction of regularly spaced and often overlapped serial sections proceeds from rostral to caudal along the neuraxis, with longitudinal alignment on the dorsomedial peak of the dorsal pallium in each section. Each reconstruction is from a single case that approximated the average values of pallial volume, surface area and thickness for its ablation and age group. The dorsal pallium is depicted as solid black in each section. Developmental effects are shown by differences in the vertical sequences, with superimposed ablation effects shown by differences in horizontal pairs from same-age littermates. Paired reconstructions are arranged as mirror images to best uncover ablation-associated asymmetry (note the mirrored directional legends for wild-type versus ablated mice). Growth of the dorsal pallium is associated with age in both control and ablated mice. However, the extent of growth is greater in control than in ablated mice throughout this developmental sequence. Directional legends: R, rostral; C, caudal; M, medial; L, lateral; V, ventral; D, dorsal.

longitudinal study. The PP, as defined by settled GPT neurons, was slowly infiltrated by cortical plate neurons from E13–E15 (Figures 5A and 5B), then persisted mainly as an SP (subplate) deep to the layer VI fibre band (Altman's channel II) (Bayer and Altman, 1991). The cortical plate consisted of early–formed proximal [CP/P (cortical plate/proximal division); infragranular layers V and VIA] and late-formed distal divisions [CP/D (cortical plate/distal division); granular and supragranular layers IV–II].

Growth defects of the dependent variable thickness were detected in all laminae of unscarred pallium in ablated mice

© 2010 The Author(s) This is an Open Access article distributed under the terms of the Creative Commons Attribution Non-Commercial Licence (http://creativecommons.org/licenses/by-nc/2.5/) which permits unrestricted non-commercial use, distribution and reproduction in any medium, provided the original work is properly cited.

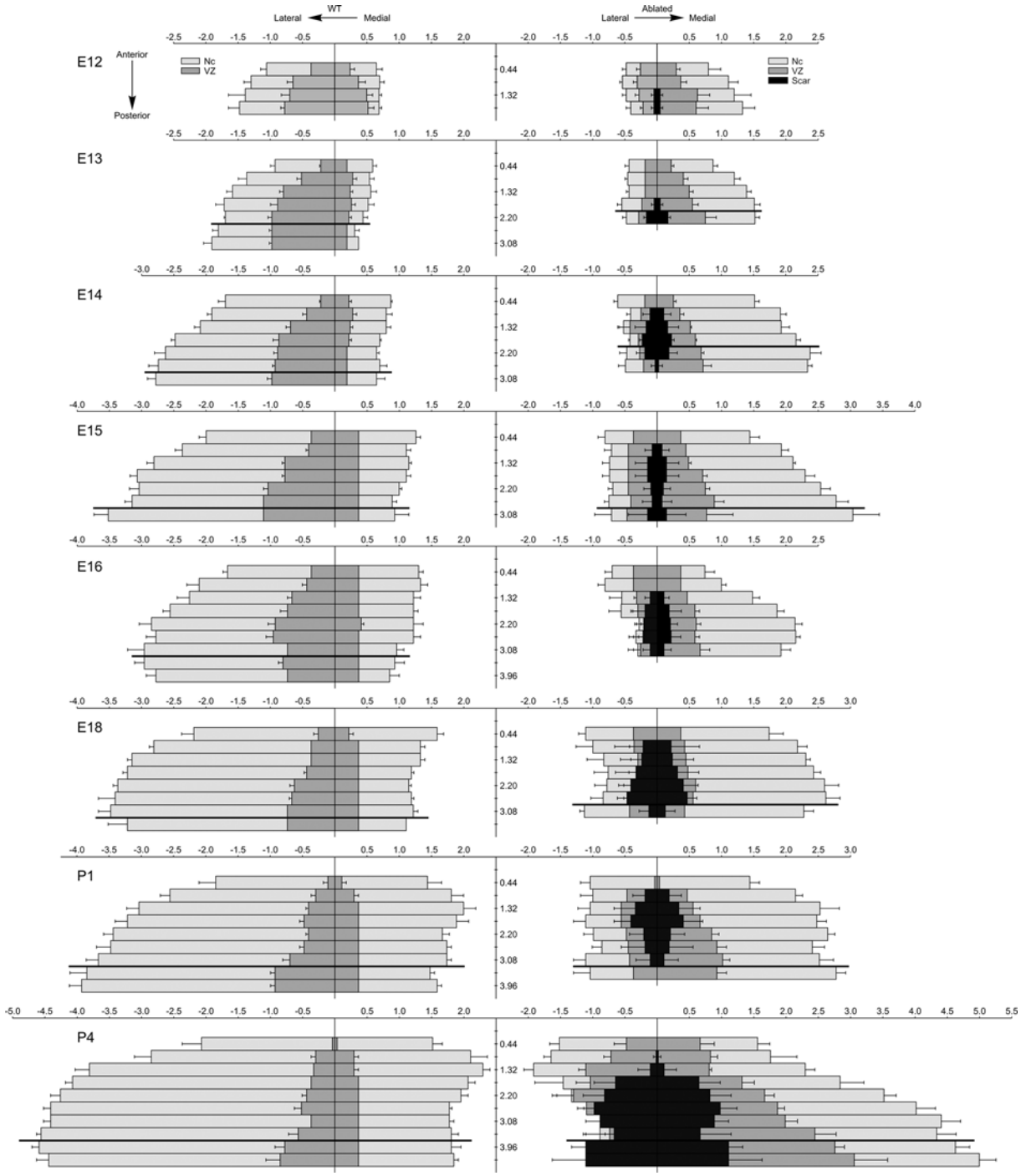

Figure 4 **Surface area maps (light grey) from serial section reconstructions in the coronal plane of the dorsal pallium in wild-type (control; left) and ablated (right) mice from E12 (top) to P4 (bottom)**

These results represent the longitudinal time-series study where four ganciclovir treatments were administered on E11–E12. Each serial reconstruction proceeds from rostral to caudal along the neuraxis (rostral vertical scale value=0), with longitudinal alignment on the dorsomedial peak of the pallium in each section (horizontal scale value=0). Each reconstruction is a compilation of the mean $\pm$ S.E.M. ($\overline{X} \pm$ S.E.M.) length of the measured surfaces of comparable, axially positioned sections drawn from all cases in each ablation and age group (three to five mice per group). Representative sections were available in each case for each group at positions anterior to the level of the dark horizontal line on each map. Surface area maps (dark grey) from the dorsal pallial VZ/SVZ are similarly generated and aligned. In ablated mice, surface area maps for pallial scars (black) are similarly generated and aligned. In ablated mice, the total surface area of the dorsal pallium included scarred and unscarred values summed across the sections. The unscarred surface area of the dorsal pallium excluded the scars from the summation. Developmental effects are shown by differences in vertical sequences, with superimposed ablation effects shown by differences in horizontal pairs from the same-age control and

© 2010 The Author(s) This is an Open Access article distributed under the terms of the Creative Commons Attribution Non-Commercial Licence (http://creativecommons.org/licenses/by-nc/2.5/) which permits unrestricted non-commercial use, distribution and reproduction in any medium, provided the original work is properly cited.

ablated groups. Paired reconstructions are arranged as mirror images to best uncover ablation-associated asymmetry. Growth of the surface areas of the dorsal pallium and its VZ/SVZ is associated with age in both control and ablated mice. However, the extent of growth is greater in control than in ablated mice throughout this developmental sequence. Note the central placement of scars at the dorsomedial peak of the pallium in ablated mice throughout the sequence, and the dramatic expansion of scars after P1.

in the longitudinal study. Figures 6(A)–6(F) show laminar thicknesses for unscarred pallium in control and ablated mice. Two-way ANOVAs demonstrated the overall statistical significance of *ablation* and *age* main effects, and the *ablation* × *age* interaction, on the thickness of each lamina between E12–P4 ($F = 16.2–388.9$; df as in previous two-way ANOVAs; $P_\alpha < 0.01$). Thickness increased with age for all laminae in control and ablated mice except the VZ/SVZ, where thickness increased then decreased with age due to early elaboration and subsequent exhaustion of the proliferative matrix (Figure 6A). Growth of the thickness of all laminae was progressively reduced in ablated mice. Relative magnitudes of differences of laminar thickness between control and ablated mice were always least in the marginal zone, and greatest in the IZ after E18. Most trends for laminar thickness had significant departures from the linearity assumption used by ANOVA models. The model was robust with regard to such violations, and its results were, for the most part, validated graphically by reliable differences between same-age control and ablated mice. Yet, such non-linear trends precluded comparisons of ANOVA coefficients of determination and growth rates obtained by linear regression.

Defective laminar growth was associated with increased cell density in the unscarred pallium of ablated mice. Within the neocortex proper (PP/SP, CP/P and CP/D), the majority of the cells were neurons derived from the underlying VZ/SVZ for the E12–P4 study period. Thus, persistent excess density reflected defective growth of the neuropil, not the somatic cellular, tissue compartment. Figures 7(A)–7(F) show laminar cell densities of unscarred pallium for control and ablated mice in the longitudinal study. Two-way ANOVAs demonstrated the overall statistical significance of *ablation* and *age* main effects, and the *ablation* × *age* interaction, on laminar cell densities between E12 and P4 ($F = 15.8–1000.9$; df as in previous two-way ANOVAs; $P_\alpha < 0.01$). Cell densities were often U-shaped functions of age in control and ablated mice. Cell densities in ablated mice attained reliably greater peak values, followed by slower decreases, than cell densities in control mice. The sequence of early, nonlinear changes of cell densities in VZ/SVZ, IZ and PP/SP of ablated mice reflected early compensatory changes of the proliferative matrix, which resulted from the generation, then replacement, of killed GPT cells. Impaired entrance, outgrowth and elaboration of axons and dendrites reduced subsequent growth in the neuropil compartment of ablated mice, which led to higher cell densities in its more mature laminar components and, for the most part, obscured the columnar organization of sensory neocortex as seen on and after E18 in control mice. As for laminar thickness, many trends for cell density departed from the ANOVA assumption of linearity, so comparisons of ANOVA coefficients of determination and growth rates from linear regression were not pursued.

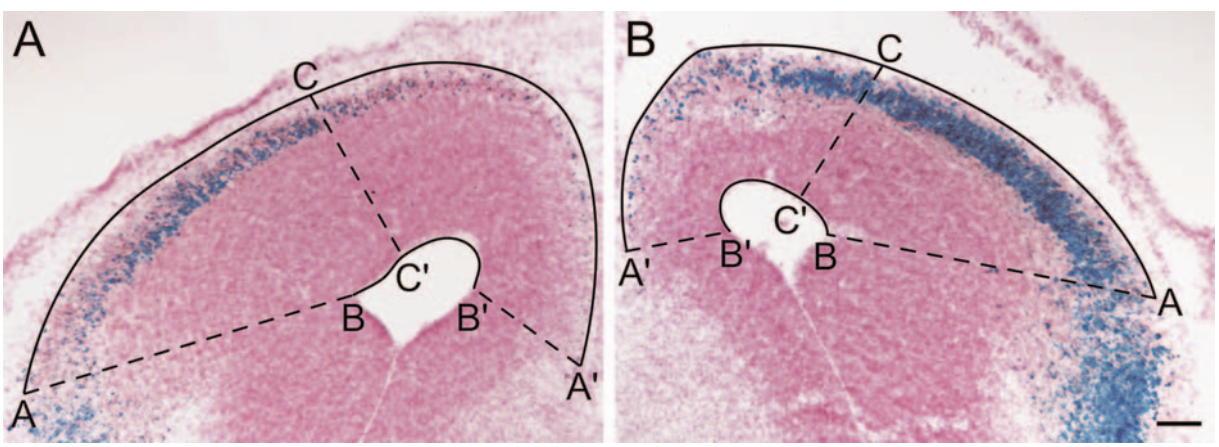

Figure 5 **Photomicrographs demonstrating the organization of GPT neurons (blue, lacZ) in coronal sections of dorsal pallium counterstained with Neutral Red in wild-type (control) (A) and littermate ablated (B) mice on E14 after four ganciclovir treatments on E11–E12**

Ablation effects are shown by differences between the representative sections, arranged as mirror images to best uncover asymmetry. In each panel, line C-C′ represents the thickness of dorsal pallium. Line A-A′ represents the surface length (at the pial interface) used to calculate the surface areas for dorsal pallium from serial section reconstructions. Line B-B′ represents the surface length (at the lateral ventricular lumen) used to calculate the surface areas for VZ/SVZ of pallium from serial section reconstructions. Line A-A′-B-B′ represents the perimeter used for planimetric calculation of volumes of pallium from serial section reconstructions. All of these lengths and areas are greater in the control mouse than in the ablated mouse. The density of GPT neurons in the dorsal pallium appears to be greater in the ablated mouse than in the control mouse; however, estimates of total frequencies of GPT neurons in the dorsal pallium as a whole are nearly equivalent in the ablated and control mice. Scale bar, 50 μm.

© 2010 The Author(s) This is an Open Access article distributed under the terms of the Creative Commons Attribution Non-Commercial Licence (http://creativecommons.org/licenses/by-nc/2.5/) which permits unrestricted non-commercial use, distribution and reproduction in any medium, provided the original work is properly cited.

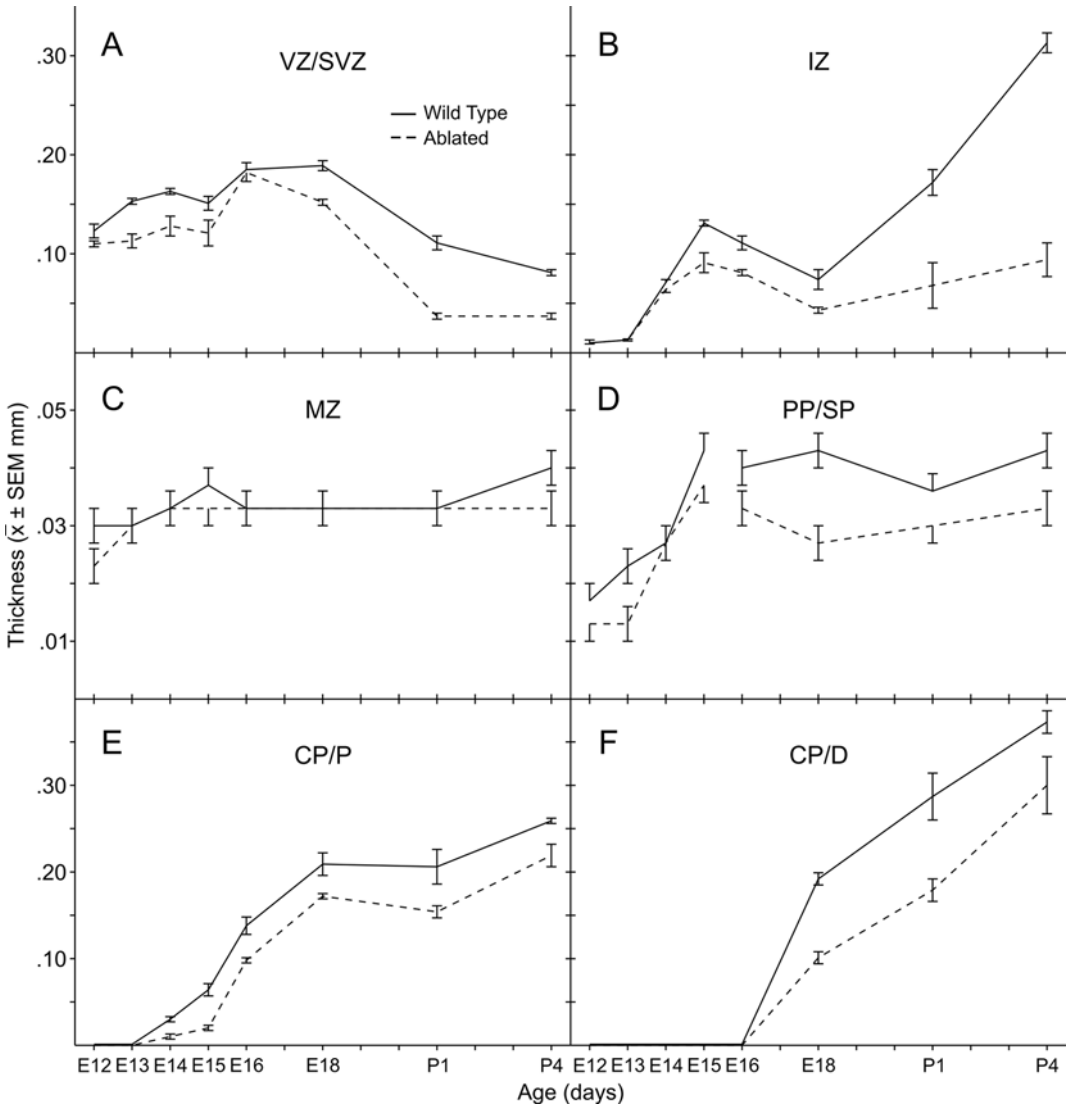

Figure 6 **Mean thickness ($\bar{X} \pm$S.E.M.) of the various laminae (A–F) constituting the unscarred dorsal pallium in wild-type (control) and ablated mice plotted as a function of age from E12 to P4**

These results represent the longitudinal time-series study where four ganciclovir treatments were administered on E11–E12. Each lamina has a distinct pattern of development. The break in the trends depicted in (**D**) represents a shift in the disposition of GPT neurons from the unilaminar PP stage of neocortex to the trilaminar immature stage of neocortex. Two-way ANOVAs demonstrate the statistical reliability of *ablation* and *age* main effects, and the *ablation* × *age* interaction, for overall comparisons of thickness between control and ablated mice in all laminae for this developmental period ($P_\alpha < 0.01$, one-tailed tests). Student's *t* tests and non-overlapped $\bar{X}$+S.E.M. demonstrate the statistical reliability of differences between pairwise contrasts of data from individual age groups for each lamina ($P_\alpha < 0.05$, one-tailed tests). The thickness of VZ/SVZ decreases with age in control and ablated mice due to exhaustion of the proliferative matrices (**A**). The thickness of IZ increases with age in control and ablated mice due to the outward radial migration of newly proliferated neurons into the neocortex followed by the establishment of axonal projections (**B**). The thickness of all other laminae increases with age in control and ablated mice due to the migration/settlement of neurons, establishment of axonal projections/terminal fields and outgrowth of neuronal dendrites/local axons (**C**–**F**). With increasing age, the thickness of all laminae in control mice tends to become greater than that in ablated mice. These differences are least apparent from E12 to P4 in the marginal zone (**C**), and most apparent in the late IZ (**B**). MZ: marginal zone (**C**); PP/SP: preplate/sublate (**D**).

Longitudinal study of growth reductions in VZ/SVZ of the dorsal pallium in ablated mice

VZ/SVZ was the main proliferative neuroepitehlial matrix for the pallium. Pallial defects in ablated mice originated from this matrix because the ablation was directed against proliferating GPT neuroblasts that were entirely located therein. This component also deserved close attention because the ventricular surface area of VZ/SVZ was an important contributor to measurements of pallial volume. Figures 8(A)-8(C) shows dependent variables of volume, area (ventricular/deep surface) and thickness of VZ/SVZ plotted against age groups and compared between ablation groups for the longitudinal study.

© 2010 The Author(s) This is an Open Access article distributed under the terms of the Creative Commons Attribution Non-Commercial Licence (http://creativecommons.org/licenses/by-nc/2.5/) which permits unrestricted non-commercial use, distribution and reproduction in any medium, provided the original work is properly cited.

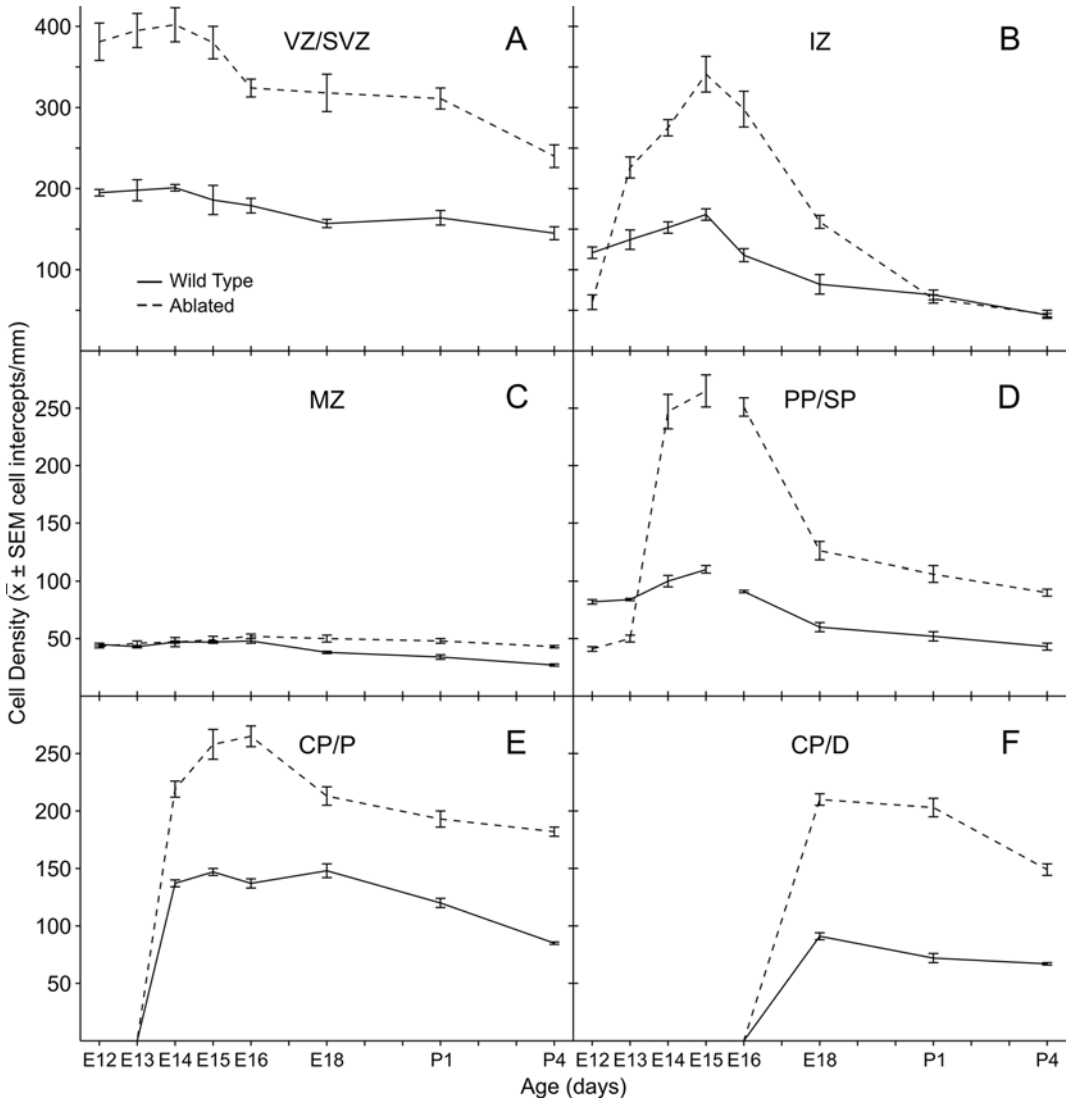

Figure 7 **Corrected mean density ($\overline{X} \pm$S.E.M.) of cells in the various laminae constituting the unscarred dorsal pallium in wild-type (control) and ablated mice plotted as a function of age from E12 to P4**

These results represent the longitudinal time-series study where four ganciclovir treatments were administered on E11–E12. Each lamina has a distinct pattern of development. The break in the trends depicted in (**D**) represents a shift in the disposition of GPT neurons from the unilaminar PP stage of neocortex to the trilaminar immature stage of neocortex. Two-way ANOVAs demonstrated the statistical reliability of *ablation* and *age* main effects, and the *ablation* × *age* interaction, for overall comparisons of cell density between control and ablated mice in all laminae for this developmental period (P_α<0.01, one-tailed tests). Student's *t* tests and non-overlapped $\overline{X}$+S.E.M. demonstrate the statistical reliability of differences between pairwise contrasts of data from individual age groups for each lamina (P_α<0.05, one-tailed tests). The cell density of VZ/SVZ decreases with age in control and ablated mice due to the exhaustion of the proliferative matrices (**A**). The cell density of IZ increases and then decreases with age in control and ablated mice due to the outward radial migration of newly proliferated neurons into the neocortex (**B**). The cell density of all other laminae tends to increase and then decrease with age in control and ablated mice due to the early migration and settlement of neurons, followed by the later expansion of the neuropil and axonal projections. The cell density of all laminae in ablated mice tends to become greater than in control mice. These differences are least apparent in the marginal zone (**C**) and are most apparent in the VZ/SVZ (**A**) for the entire E12–P4 period of development. MZ, marginal zone (**C**); PP/SP, preplate/sublate (**D**).

Two-way ANOVAs demonstrated the overall statistical significance of *ablation* and *age* main effects, and the *ablation* × *age* interaction, on the volume, area and thickness of pallial VZ/SVZ between E12 and P4 (**F**=10.3–125.9; df as in previous two-way ANOVAs; P_α<0.01), except for the *ablation* main effect on VZ/SVZ total area (**F**=0.2; df=1,64; P_α>0.01). Growth of all dependent variables usually occurred as non-linear U-shaped functions of age in control and ablated mice, which reflected the expansion and subsequent exhaustion of the proliferative matrix, and the migratory exit of newly generated, non-mitotic neurons. This characterization did not apply to growth of VZ/SVZ total and unscarred areas in

© 2010 The Author(s) This is an Open Access article distributed under the terms of the Creative Commons Attribution Non-Commercial Licence (http://creativecommons.org/licenses/by-nc/2.5/) which permits unrestricted non-commercial use, distribution and reproduction in any medium, provided the original work is properly cited.

ablated mice after E18, when progressive hydrocephalus stretched the ventricular surface (Figure 8B) and destroyed the ependymal cell layer. Compared with control mice, VZ/SVZ growth was reliably reduced in ablated mice, and reductions became progressively more severe with age. Graphic comparisons between control and ablated mice at each age level showed reliable differences between groups, which were usually statistically significant for all three dependent variables on and after E12. These differences preceded by one day (24 h) the set of related, reliable reductions for volume, area and thickness in the pallium as a whole (Student's *t* tests; df=6–8; $P_\alpha<0.05$).

As for comparable dependent variables for the pallium, the trends for all three dependent variables in the VZ/SVZ in ablated mice had early deflections that reflected stalled growth, but not tissue loss, between E11 and E13. Late deflections also occurred between E15 and E16 for volumes and surface areas in ablated mice, which might have reflected a residual defect in the final separation of SVZ from VZ (Figure 8; Bayer and Altman, 1991). Trends obtained for all dependent variables in the VZ/SVZ from E12–P4 departed significantly from the assumption of linearity used by ANOVA models, so ANOVA coefficients of determination and growth rates from linear regression were not calculated for the full study period. However, the assumption of linearity was better approximated between E12 and E18, the principal period of proliferation for pallial neurons and the limited age range employed for further analysis.

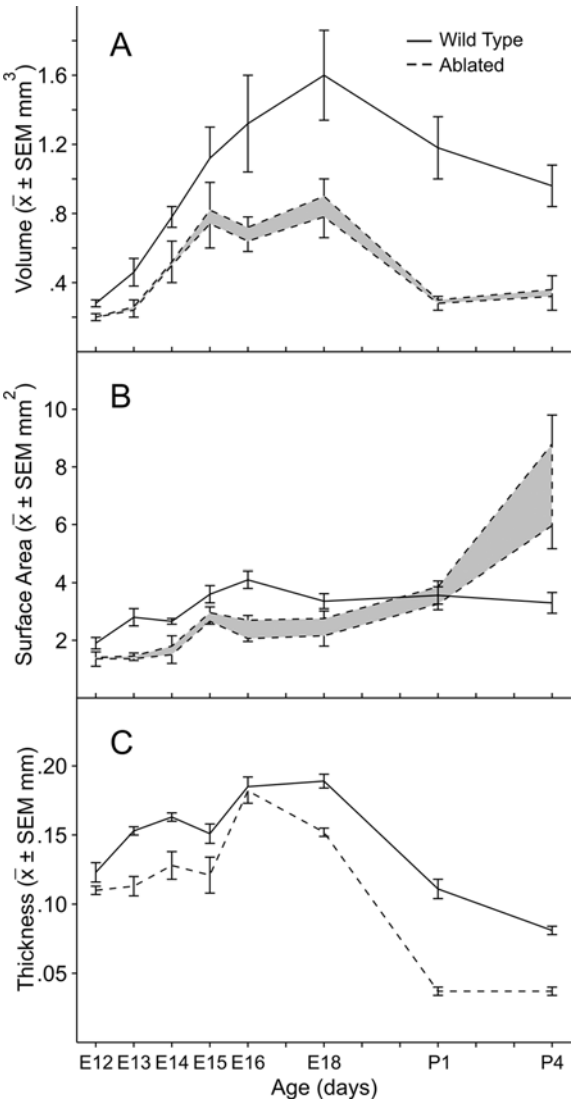

Figure 8 Mean volume (A), surface area (at lateral ventricular lumen) (B) and thickness (C) ($\bar{X}\pm$S.E.M.) of the VZ/SVZ of the dorsal pallium in wild-type (control) and ablated mice plotted as a function of age from E12 to P4

These results represent the longitudinal time-series study where four ganciclovir treatments were administered on E11–E12. For ablated mice in (**A**) and (**B**), the upper trends represent $\bar{X}$+S.E.M. total (scarred plus unscarred) volumes and surface areas, whereas the lower trends represent $\bar{X}-$S.E.M. unscarred volumes and surface areas. Shaded areas between upper and lower trends for ablated mice represent scarred VZ/SVZ in the dorsal pallium. Two-way ANOVAs demonstrate the statistical reliability of *ablation* and *age* main effects, and the *ablation* × *age* interaction, for most overall comparisons between control and ablated mice during this developmental period on each measure of volume, surface area and thickness ($P_\alpha<0.01$, one-tailed tests). The assumption of linearity was met from E12 to E18, corresponding to the activity of the proliferative matrix, but was not fulfilled for the entire period. Student's *t* tests and non-overlapped $\bar{X}$+S.E.M. demonstrate the statistical reliability of differences between pairwise contrasts of data from individual age groups ($P_\alpha<0.05$, one-tailed tests).

Quantitative volume defects in VZ/SVZ

VZ/SVZ volume in control mice increased from 0.28 ± 0.04 mm^3 ($\bar{X}\pm$S.E.M.) to 1.60 ± 0.52 mm^3 between E12 and E18, a measured cumulative growth of 471% (calculated from E18-E12/E12 values; Figure 8A). Volume was reliably correlated with age (**r**=0.79; df=26; $P_\alpha<0.05$) with a growth rate of 0.24 mm^3/day. The predicted E11 volume (0.18 mm^3) yielded a cumulative growth of 789% (E18–E11/E11 values). VZ/SVZ total volume in ablated mice increased from 0.20 ± 0.02 to 0.90 ± 0.10 mm^3 between E12 and E18, a measured cumulative growth of 350%. The total volume was reliably correlated with age (**r**=0.77; df=28; $P_\alpha<0.05$) with a growth rate of 0.12 mm^3/day, half of the control value. The predicted E11 total volume (0.18 mm^3, the predicted E11 control value) yielded a cumulative growth of 400% in ablated mice. At E18, the predicted total volume in ablated mice was 51% of the control value, consistent with an observed reduction to 56% (i.e. a 44% growth shortfall).

VZ/SVZ unscarred volume in ablated mice increased from 0.20 ± 0.02 to 0.79 ± 0.13 mm^3 between E12 and E18, a measured cumulative growth of 295%. Unscarred volume was reliably correlated with age (**r**=0.73; df=28; $P_\alpha<0.05$) with a growth rate of 0.10 mm^3/day, less than half of the control value. The predicted E11 unscarred volume (0.18 mm^3) yielded a cumulative growth of 339% in ablated mice. At E18, the predicted unscarred volume in ablated mice was 43% of the control value, nearly identical with an observed reduction to 44% (a 56% growth shortfall).

© 2010 The Author(s) This is an Open Access article distributed under the terms of the Creative Commons Attribution Non-Commercial Licence (http://creativecommons.org/licenses/by-nc/2.5/) which permits unrestricted non-commercial use, distribution and reproduction in any medium, provided the original work is properly cited.

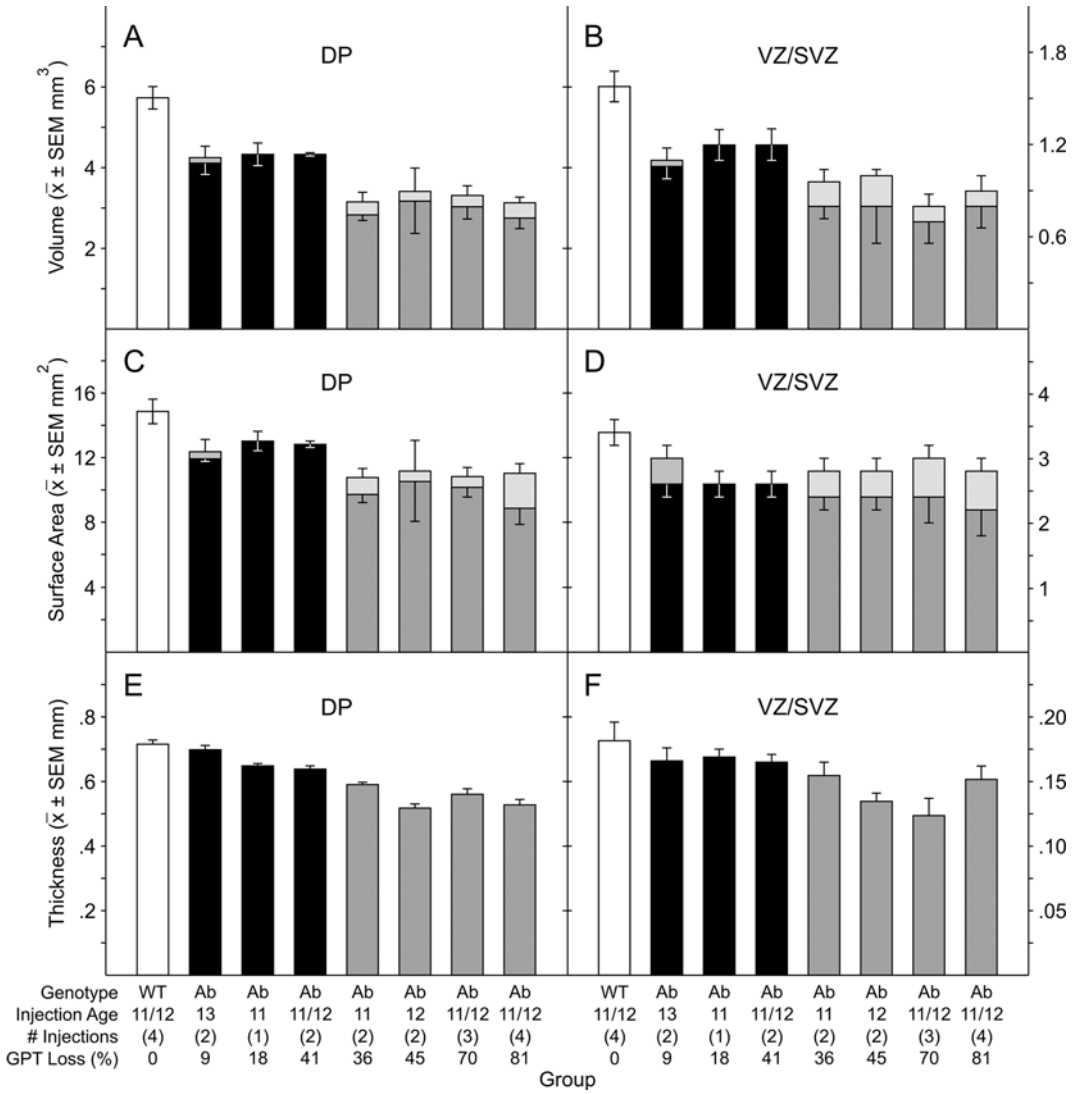

Figure 9 **Mean volume (A, B), surface area (at the pial interface and lateral ventricular lumen respectively; C, D) and thickness (E, F; $\bar{X}\pm$S.E.M.) of the dorsal pallium (A, C, E) and the VZ/SVZ of the dorsal pallium (B, D, F) in wild-type (control) and ablated mice plotted for various ablation groups terminated on E18**

These results represent the cross-sectional study where genotypes, ages at ganciclovir treatment, frequency of ganciclovir treatments and calculated percentage extent of GPT cell loss are displayed on the *x*-axis. For ablated mice (**A–D**), the upper bar limits represent $\bar{X}$+S.E.M. total (scarred plus unscarred) volumes and surface areas, whereas the lower bar limits represent $\bar{X}-$S.E.M. unscarred volumes and surface areas respectively. Shaded areas between upper and lower bar limits for ablated mice represent scarred dorsal pallium or its scarred VZ/SVZ. One-way ANOVAs demonstrate the statistical reliability of the *ablation* effect for overall comparisons of each measure of volume, area and thickness between control and ablated mice at this developmental benchmark ($P_\alpha<0.01$, one-tailed test). White bars represent the 'control' cluster of groups [wild-type (WT) controls], black bars represent the 'mild ablation' cluster of groups and grey bars represent the 'severe ablation' cluster of groups. One-way ANOVAs demonstrated the statistical reliability of most differences between these clusters on the various measures (see the Results section for exceptions; $P_\alpha<0.01$, one-tailed tests). The control cluster typically had greater values than the mild and severe ablation clusters. The mild ablation cluster typically had greater values than the severe ablation cluster. Student's *t* tests and non-overlapped $\bar{X}$+S.E.M. demonstrate the statistical reliability of differences between pairwise contrasts of grouped data ($P_\alpha<0.05$, one-tailed tests).

VZ/SVZ scars were observed on and after E13 in all ablated, and no control, mice in the longitudinal study. Scar volume increased from 0.02 ± 0.01 to 0.11 ± 0.02 mm^3 from E13–P1, a cumulative growth of 450%. The scar volume growth rate of 0.01 mm^3/day was less than 10% of the growth rate for adjacent, unscarred VZ/SVZ. Scars were less than 10% of VZ/SVZ volume throughout the full E12–P4 study period.

Quantitative area defects in VZ/SVZ

VZ/SVZ area in control mice increased from 1.90 ± 0.20 to 3.30 ± 0.36 mm^2 between E12 and E18, a measured cumulative growth of 73% (Figure 8B). Area was reliably correlated with age ($r=0.56$; df=26; $P_\alpha<0.05$) with a growth rate of 0.30 mm^2/day. The predicted E11 area (1.36 mm^2) yielded a cumulative growth of 142%.

© 2010 The Author(s) This is an Open Access article distributed under the terms of the Creative Commons Attribution Non-Commercial Licence (http://creativecommons.org/licenses/by-nc/2.5/) which permits unrestricted non-commercial use, distribution and reproduction in any medium, provided the original work is properly cited.

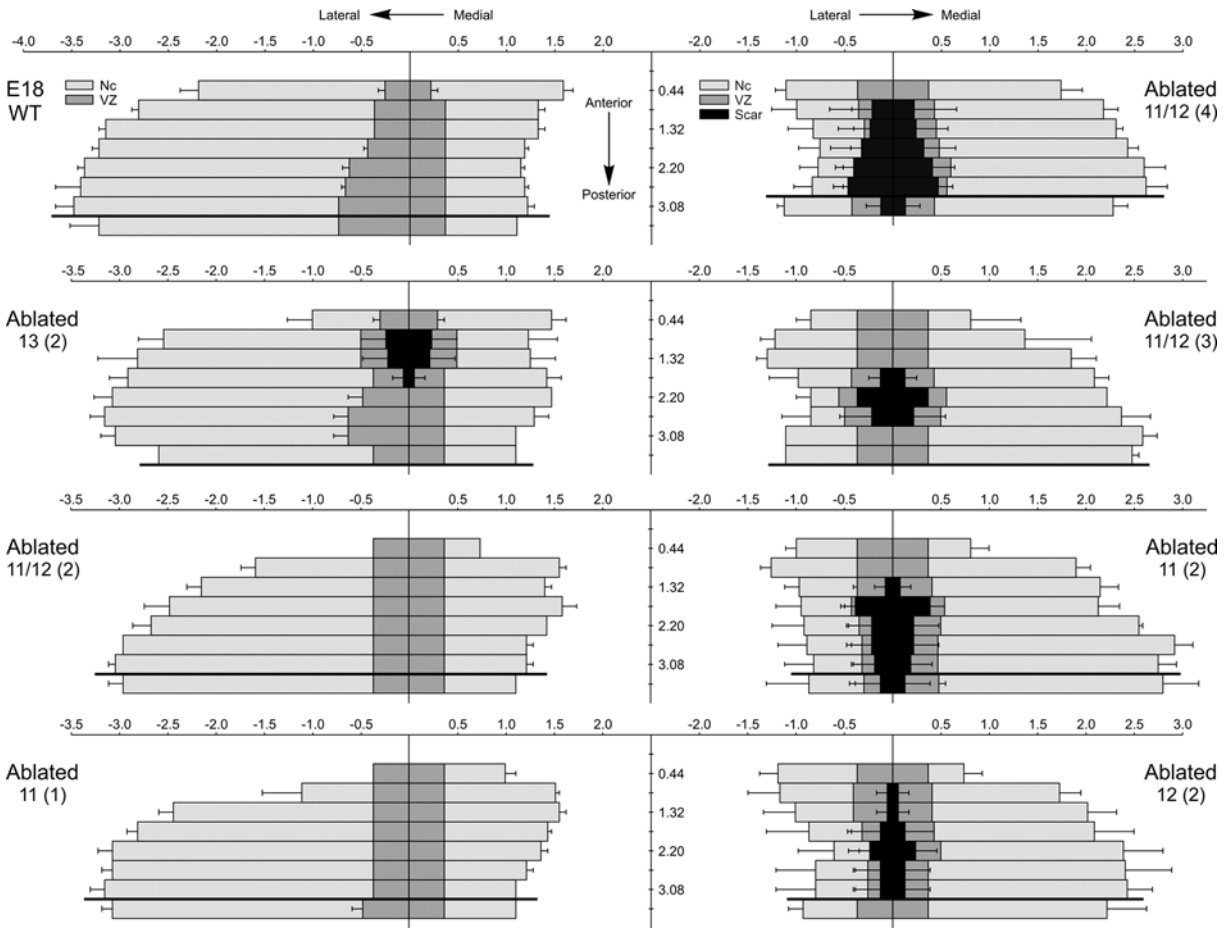

Figure 10 **Surface area maps (light grey) from serial section reconstructions in the coronal plane of the dorsal pallium in wild-type (control; left) and ablated (right) mice plotted for various ablation groups terminated on E18**

These results represent the cross-sectional study. Each serial reconstruction is produced as in Figure 4, and proceeds from rostral to caudal along the neuraxis (rostral vertical scale value=0), with longitudinal alignment on the dorsomedial peak of the pallium in each section (horizontal scale value=0). Each reconstruction is a compilation of the mean $\pm$ S.E.M. ($\bar{X} \pm$ S.E.M.) length of the measured surfaces of comparable, axially positioned sections drawn from all cases in each ablation and age group (3–10 mice per group). Representative sections were available in each case for each group at positions anterior to the level of the dark horizontal line on each map. Surface area maps (dark grey) from the dorsal pallial VZ/SVZ are similarly generated and aligned. In ablated mice, surface area maps for pallial scars (black) are similarly generated and aligned. In ablated mice, the total surface area of dorsal pallium included scarred and unscarred values summed across the sections. The unscarred surface area of the dorsal pallium excluded the scars from the summation. Developmental effects are shown by differences in vertical sequences, with superimposed ablation effects shown by differences in horizontal pairs from same-age control and ablated groups. Paired reconstructions are arranged as mirror images to best uncover ablation-associated asymmetry. The ablated groups tend to have smaller surface areas when compared with the control group. Groups in the severe ablation cluster (right-hand side maps) tend to have smaller surface areas when compared with mice in the mild ablation and control clusters (left-hand side maps).

VZ/SVZ total area in ablated mice increased from 1.40 ± 0.20 to 2.76 ± 0.26 mm^2 between E12–E18, a cumulative growth of 97%. Total area was reliably correlated with age ($r=0.71$; df=28; $P_\alpha<0.05$) with a growth rate of 0.28 mm^2/day, slightly less than the control value. The predicted E11 total area (1.36 mm^2) yielded a cumulative growth of 102% in ablated mice. At E18, the predicted total area in ablated mice was 72% of the control value, slightly less than an observed reduction to 82% (an 18% growth shortfall, considerably reduced by the initiation of hydrocephalic expansion).

The VZ/SVZ unscarred area in ablated mice increased from 1.36 ± 0.26 to 2.16 ± 0.36 mm^2 between E12 and E18, a cumulative growth of 59%. Unscarred area was reliably correlated with age ($r=0.53$; df=28; $P_\alpha<0.05$) with a growth rate of 0.16 mm^2/day, less than 60% of the control value. The predicted E11 unscarred area (1.36 mm^2) yielded a cumulative growth of 59% in ablated mice. At E18, the predicted unscarred area in ablated mice was 41% of the control value, considerably less than an observed reduction to 66% (a 34% growth shortfall, modestly reduced by the initiation of hydrocephalic expansion).

© 2010 The Author(s) This is an Open Access article distributed under the terms of the Creative Commons Attribution Non-Commercial Licence (http://creativecommons.org/licenses/by-nc/2.5/) which permits unrestricted non-commercial use, distribution and reproduction in any medium, provided the original work is properly cited.

Scar area increased from 0.10 ± 0.02 to 0.60 ± 0.10 mm^2 between E13 and E18, a cumulative growth of 500%. The scar area growth rate of 0.07 mm^2/day was less than 44% of the growth rate for adjacent, unscarred VZ/SVZ. Scars were less than 22% of VZ/SVZ total area in ablated mice until P1, followed by expansion to 33% on P4.

Quantitative thickness defects in the VZ/SVZ

VZ/SVZ thickness in control mice increased from 0.123 ± 0.007 to 0.189 ± 0.005 mm between E12 and E18, a cumulative growth of 54% (Figure 8C). Thickness was reliably correlated with age (**r**=0.77; df=26; $P_\alpha<0.05$) with a growth rate of 0.009 mm/day. The predicted E11 thickness (0.110 mm) yielded a cumulative growth of 72%.

VZ/SVZ thickness in ablated mice increased from 0.110 ± 0.003 to 0.152 ± 0.006 mm between E12 and E18, a cumulative growth of 38%. Thickness was reliably correlated with age (**r**=0.61; df=28; $P_\alpha<0.05$) with a growth rate of 0.006 mm/day, less than 66% of the control value. The predicted E11 thickness (0.110 mm) yielded a cumulative growth of 38% in ablated mice. At E18, the predicted thickness in ablated mice was 63% of the control value, somewhat less than an observed reduction to 80% (a 20% growth shortfall).

Interrelationships of volume, area and thickness in VZ/SVZ

VZ/SVZ volume, area and thickness had reliable intercorrelations between the dependent variables, which demonstrated their substantial internal validity from E12 to E18. For VZ/SVZ in control mice, the values for **r**=0.79 (volume versus area), 0.71 (volume versus thickness) and 0.55 (area versus thickness; df=26; $P_\alpha<0.05$). For total VZ/SVZ in ablated mice, the respective values for **r**=0.86, 0.62 and 0.49 (df=28; $P_\alpha<0.05$). For unscarred VZ/SVZ in ablated mice, the respective values for **r**=0.49, 0.75 and 0.59 (df=28; $P_\alpha<0.05$). For each pair of dependent variables, intercorrelations were less for VZ/SVZ than for whole pallium, whether considered for E12–E18 or E12–P4 periods.

Interrelationships between growth in VZ/SVZ and pallium

Reliable intercorrelations were observed between related dependent variables for the VZ/SVZ and pallium during the E12–E18 period. VZ/SVZ and pallium volumes were reliably correlated in control mice (**r**=0.96; df=26), VZ/SVZ and pallium total volumes were reliably correlated in ablated mice (**r**=0.92; df=28), and VZ/SVZ and pallium unscarred volumes were reliably correlated in ablated mice (**r**=0.89; df=28; $P_\alpha<0.05$). Similar results were obtained for VZ/SVZ area and thickness despite their weaker correlations with age. Respectively comparable values for areas were **r**=0.80 (df=26; control areas); **r**=0.92 (df=28; ablated total areas); and **r**=0.89 (df=28; ablated unscarred areas; $P_\alpha<0.05$). Finally, VZ/SVZ and pallium thicknesses were reliably correlated in control mice (**r**=0.81; df=26) and in ablated mice (**r**=0.73; df=28; $P_\alpha<0.05$). Between E12 and E18 in control and ablated mice, the pallium and its VZ/SVZ accumulated the proliferative output of VZ/SVZ from the *preceding* day of maturation, which accounted for their comparable and coincidental relative growth.

VZ/SVZ was the predominant component of pallium during the early study period, but was reduced to a minor contribution near its end. VZ/SVZ typically retained its proportional developmental relationships with pallium despite ablation. At E12 in control mice, the average VZ/SVZ volume was 61% of the average pallial volume and decreased to 7% by P4. At E12 in ablated mice, volumes for total and unscarred VZ/SVZ were 56% of volumes of total and unscarred pallium and decreased to 5% at P4. At E12 in control mice, VZ/SVZ area was 54% of pallial area and decreased to 13% at P4. At E12 in ablated mice, areas for total and unscarred VZ/SVZ were 48 and 50% respectively of areas for total and unscarred pallium, decreased with age until after E18 and then expanded by progressive hydrocephalus to 46 and 41% at P4. At E12 in control mice, VZ/SVZ thickness was 60% of pallial thickness and decreased to 7% by P4. At E12 in ablated mice, VZ/SVZ thickness was 58% of pallial thickness and decreased to 6% at P4.

Cross-sectional study of growth reduction in dorsal pallium and VZ/SVZ of ablated mice

The final opportunity to observe the developmental effects of the ablation of GPT neurons on growth, unalloyed by myelination and hydrocephalus, occurred on E18 after all ablated mice in the various ganciclovir treatment groups entered the third phase of secondary, late-onset apoptosis. Mice in the control group had significantly greater volume, area and thickness of both pallium and VZ/SVZ than mice pooled across ablation groups, regardless of the presence or absence of scars (Figure 9; Student's *t* tests; df=35; $P_\alpha<0.05$). Thus all effective genetically targeted ablations of GPT neurons had a persistent, negative impact on pallial growth, as in the longitudinal study. However, experimental mice with ganciclovir treatments on E14, E15 and E17 had ineffective (i.e. no) ablations. Their values were closely comparable with those of the control group on all measures, so they were excluded from further analysis.

The ablation phenotype was predicated on the specific killing of GPT cells, which was now shifted explicitly to the status of a ratio scale-independent variable in order to assess its association with downstream indicators of physical growth (dependent variables of volume, area and thickness of the pallium and its VZ/SVZ). When cases were grouped on the basis of derived percentage reductions of GPT neurons (i.e. the original, total complement of GPT neurons normally generated on E11–E13), one-way ANOVAs demonstrated that the quantified *ablation* effect still had a reliable, negative, overall impact on the E18 values attained by all dependent variables (**F**=5.68–26.72; df=7,29; $P_\alpha<0.01$) except the total VZ/SVZ

© 2010 The Author(s) This is an Open Access article distributed under the terms of the Creative Commons Attribution Non-Commercial Licence (http://creativecommons.org/licenses/by-nc/2.5/) which permits unrestricted non-commercial use, distribution and reproduction in any medium, provided the original work is properly cited.

surface area (**F**=3.16; df=7,29; P_α>0.01). The overall ablation effect was sufficiently robust to permit linear regression between the treatment groups, including the zero baseline value of the control group. Derived percentage reductions of GPT neurons were reliably but negatively correlated with the values attained by all dependent variables (i.e. less reduction produced more growth; for volume, area and thickness for pallium and VZ/SVZ, the range of values for **r** was −0.35 to −0.84; df=35; P_α<0.05). The overall dose–response relationships between the magnitudes of ablations and subsequent cumulative growth generated correlations that accounted for substantial portions of variance obtained for all pallial and VZ/SVZ dependent variables (the range of values for $\mathbf{r}^2$ was 0.43–0.71) except for VZ/SVZ total area ($\mathbf{r}^2$=0.13).

Unlike the E11–E13 stage of GPT cell killing by ganciclovir treatment, this later dose–response relationship had additional constraints as shown in Figure 9. By E18, similar outcomes in different treatment groups formed three natural, step-like clusters for all dependent variables: a 'control' cluster (composed of the wild-type control group) with the largest values, a 'mild ablation' cluster (composed of experimental groups with single ganciclovir treatments on E11 and E12, one ganciclovir treatment on E11 and two ganciclovir treatments on E13) with intermediate values, and a 'severe ablation' cluster (composed of experimental groups with four ganciclovir treatments on E11–E12, three ganciclovir treatments on E11–E12, two ganciclovir treatments on E12 and two ganciclovir treatments on E11) with the least values. One-way ANOVAs revealed a reliable *ablation* effect between the three clusters for all dependent variables in pallium and VZ/SVZ (**F**=10.19–69.66; df=2,34; P_α<0.01). Also, statistically reliable differences were obtained in contrasts between the control and severe ablation clusters, the control and mild ablation clusters, and the mild and severe ablation clusters for all dependent variables (Student's *t* tests; df=24, 19 and 25 respectively; P_α<0.05), except for the contrast of mild and severe ablation clusters for VZ/SVZ total surface area (P_α>0.05). However, unreliable or marginal differences were obtained from between-group contrasts within the severe and mild ablation clusters (P_α>0.05). As expected, the stochastic cluster arrangement indicated that genetically targeted ablations were, in fact, serial lesions, where the timing and sequence of the specific killing of GPT cells, as well as the intervening percentage reduction of GPT neurons, influenced downstream growth. This was particularly evident in the ablation group with ganciclovir intertreament intervals greater than 24 h on E11–E12, where a severe ablation of GPT neurons (41% reduction) produced mild growth defects.

The ordered relationships between ablation groups and growth reductions in pallium observed at E18 were also demonstrated in anatomical maps. Selected because it addresses directly the issue of horizontal growth defects, Figure 10 shows the averaged, flat-mapped surface areas of the pallium, its VZ/SVZ and, when present, its scars, for the groups studied at E18. Compared with the control group, the mild ablation groups had modest and comparable reductions in pallial and VZ/SVZ areas. The severe ablation groups had greater reductions than both the control and mild ablation groups. Scars were also more common and extensive in severe ablation groups, with large scars found in association with large ablations.

DISCUSSION

The present study centres on an anatomical entity, the dorsal pallium, defined first and foremost by a neurochemical property, the localization of GPT-expressing cells (GPT neuroblasts and neurons). GPT is unusual for its early and continued expression during cell lineage progression from neuroblast to neuron stages (and its absence in other preceding or concurrent precursors invulnerable to the present genetically targeted ablation), as well as its wide horizontal extent in the pallial proliferative matrix (Osheroff and Hatten, 2009; Xie et al., 2009). It provides a novel, modern view of one of the largest structural components in mammalian brain consistent with the organizational scheme of Marin-Padilla (1971, 1998). Evidence based on this molecular marker characterizes the most dynamic phase of pallial morphogenesis in mice, but may not be strictly comparable with earlier reports based on different criteria for anatomical boundaries. Nevertheless, measurements of length, width and height of telencephalic vesicles in control mice match corresponding values from same-age examples of normal fetal mice shown by Kaufman (1992). External validation of these measurements for P4 control mice also occurs in Valverde's (1998) masterful Golgi study of P5–P7 mice. Our values are 10% less than those of Valverde, with such slight differences most probably due to the effects of cryoprotection, fixation and age. Since the new measurements of the pallial volume are reasonably accurate, revised estimates of full, hemispheric complements of 2.5×10^5 dorsal pallial GPT neurons in control mice and 2.3×10^5 dorsal pallial GPT neurons in severely ablated mice are calculated from peak developmental densities of viable GPT neurons normalized for pallial volume, with the difference due to the lost proliferative output of VZ scars (Xie et al., 2009). Genetically targeted ablation of GPT cells persistently eliminates up to 81% of the original complement of GPT neurons. The subsequent, comparable peak values demonstrate a near-normal restoration of GPT neurons tightly packed into an unscarred pallium of reduced size in ablated mice. The ablation is remarkable because the targeted cell population is transiently reduced, but not permanently suppressed.

The evidence obtained by the present study proves beyond reasonable doubt that genetically targeted ablation of GPT cells results in progressive and substantial reductions of pallial growth in prenatal mice, despite compensatory

© 2010 The Author(s) This is an Open Access article distributed under the terms of the Creative Commons Attribution Non-Commercial Licence (http://creativecommons.org/licenses/by-nc/2.5/) which permits unrestricted non-commercial use, distribution and reproduction in any medium, provided the original work is properly cited.

responses that rapidly replace the ablated cells (Xie et al., 2009). Furthermore, these growth defects originate from the proliferative matrix of the pallial VZ, in accord with the rationale of the mechanism of action of the genetically targeted ablation (Xie et al., 2002, 2009). Finally, these growth defects accumulate during prenatal and postnatal development in a constrained dose–response relationship with the extent of specific killing of GPT neurons, concordant with the purported specificity of action of the genetically targeted ablation (Xie et al., 2002, 2009). GPT neurons are, in fact, the principal PP neurons, and developmental delays caused by their early, specific killing and regeneration trigger a cascade of subsequent defects in PP, immature and mature stages of neocortex, the main derivative of the proliferative matrix of the pallial VZ (Bayer and Altman, 1991). These defects uncover biologically significant aspects of neocortical morphogenesis (determinants of organic growth and form) that are often neglected or inadequately characterized (Jacobson, 1970; Price and Willshaw, 2000).

The hypothesis that the ablation of GPT cells impairs vertical, but not horizontal, growth within the pallium and its neocortical part must be rejected. The evidence obtained by this investigation proves beyond reasonable doubt that growth falters in the horizontal surface area at both the pial and ventricular borders (as well as in the vertical thickness) of the pallium in ablated mice. Simultaneous growth defects in both the horizontal and vertical cytoarchitectural dimensions combine to produce a localized shortfall of dorsal pallial volume in the telencephalic vesicles. These findings expand and explain ambiguous, less detailed signs of impaired forebrain growth reported after ablation of GPT cells (Xie et al., 2002, 2009) and ablation of PP neurons, purportedly with spared progenitors (Ghosh and Shatz, 1993).

Three aspects of the present study are unusual and merit further attention.

Detection of organic growth defects after genetically targeted ablation

Modern combinations of molecular biology and neurochemistry such as genetically targeted ablation can provide a genuine experimental 'dissection' of embryological development through the selective elimination or enhancement of its cellular elements (Xie et al., 2002; Jacobs et al., 2009). These experiments are predicated on the subsequent, accurate recognition of alterations in phenotype. In practice, large-scale organic differences in structural phenotype can be difficult to identify and thus may be overlooked even by experienced investigators. As shown here, cursory examination is inadequate if it leads to paradoxical and potentially misleading results. We resort to antique, but not antiquated, methods of macroscopic morphometry from haematoxylin-counterstained serial section reconstructions to solve this problem by detection of pallial growth defects, and their place within a developing organic context, in ablated mice.

Serial section reconstructions at appropriate low magnifications allow all aspects of an organ to be viewed simultaneously and as a whole. Structural differences greater than 20–25% are usually needed for immediate recognition of revised phenotype. Instead, barely perceptible growth defects of less than 10% are evenly distributed across all three spatial dimensions of the ablated telencephalic vesicle. Such a widespread distribution of defects sustains the co-ordination of telencephalic and neurocranial growth, a pivotal outcome for successful prenatal development and live birth of ablated mice. Nevertheless, mapping and measurement reveal more substantial differences limited to the dorsal pallial part of the telencephalic vesicle. The volume, area and thickness of control pallium have distinct growth rates and levels of cumulative physical growth due to the different spatial dimensions that contribute to each dependent variable. These indices retain distinct, but suppressed, growth rates and levels of cumulative physical growth in ablated unscarred pallium. All three dependent variables have comparable growth defects relative to their physical magnitude despite measurement by independent means. This normalization for spatial dimensional scaling uncovers a common shortfall of growth, approx. 50% of its potential in control pallium, which propagates simultaneously as horizontal and vertical defects in ablated pallium, as shown by high intercorrelations of its volume, area and thickness.

In control mice, short-lived GPT intermediate progenitor cells in the pallial VZ are the exclusive source of its GPT neurons (Landry et al., 1998; Xie et al., 2002, 2009; Jacobs et al., 2007). Between E11 and E13, these cells migrate radially in an 'outside-in' pattern and settle as the principal constituent neurons of PP neocortex. Between E13 and E15, they are infiltrated and dispersed by proximal, inverted settlement of early cortical plate neurons (destined for layers V and VI) to form trilaminar immature neocortex. By E16, physical separation of principal PP neurons settled in marginal zone versus cortical plate (i.e. true cleavage) proceeds with distal, inverted settlement of cortical plate neurons (destined for layers II–IV) to form hexalaminar mature neocortex (Bayer and Altman, 1990, 1991). In ablated mice, cellular lamination is normally ordered in PP, immature and mature stages of neocortex. Dyslamination consists of horizontal and vertical growth defects distributed across all laminae, which are characteristically thin, densely cellular and obscurely bordered by projection axons and afferent terminal fields. The delayed settlement and tight packing of a near-normal complement of GPT neurons into this smaller ablated neocortex merely emphasize the presence of the middle lamina of principal PP neurons as usually found during its immature stage (Luskin and Shatz, 1985; Xie et al., 2009). Similar growth defects, with thin lamination and tight cell packing, are also distributed across the subcortical laminae of pallium.

Growth defects in the pallial VZ precede and are highly intercorrelated with subsequent growth defects in more distal pallial laminae. During the first phase of ablation, VZ growth

© 2010 The Author(s) This is an Open Access article distributed under the terms of the Creative Commons Attribution Non-Commercial Licence (http://creativecommons.org/licenses/by-nc/2.5/) which permits unrestricted non-commercial use, distribution and reproduction in any medium, provided the original work is properly cited.

stalls due to ganciclovir-induced cell killing, which evokes a profound structural reorganization of new GPT cells and mitotic precursors in pallial VZ. As dying cells down-size the original periventricular mitotic array, newly generated mitotic cells reconstitute as a paraventricular mitotic array (e.g. a thickened, porous plate akin to later-formed SVZ; Smart, 1973; Noctor et al., 2001; Xie et al., 2009). Despite its horizontal and vertical compaction, the reconstituted matrix increases cell density in the VZ, with a concomitant increase in proliferative output sufficient to compensate for killed GPT cells during the second phase of the ablation. The reconstituted matrix maintains the normal sequence of generation for PP, proximal and distal cortical plate neurons, and replenishes by *de novo* proliferation the normal complement of GPT neurons. The compensatory response is necessary for the resumption of pallial growth, which indicates that principal PP neurons are essential building blocks for the physical foundation of the neocortical assembly (Ghosh and Shatz, 1993). The subsequent cost of growth reduction indicates that the VZ proliferative matrix encodes, at least in part, the physical dimensions of the pallium (Rakic, 2005). The original VZ template is reduced by specific cell killing in ablated mice. The 'gathering up' of the reconstituted matrix limits the outward spread of the regenerated VZ template, diminishes the mobility of precursor and progenitor cells within it and translates into a horizontal growth defect in the somatic compartment of its neocortical derivatives (Walsh and Cepko, 1993). Concurrent destruction of radial fibres contributes to horizontal and vertical growth defects in the somatic and neuropil tissue compartments. Dying GPT neuroblasts lose their radial fibres. RC2-immunoreactive radial fibres, believed to originate from neuronal precursors but not intermediate progenitors at this stage of development (Misson et al., 1988; Hasling et al., 2003; Molyneaux et al., 2007), are then grossly reduced as ganciclovir-invulnerable, non-GPT-expressing precursors are recruited toward production of GPT neuroblasts. The decimation and disarray of the radial fibre network impair the distal disaggregation of settling neurons and reduce their migratory trajectory, but do not block radial migration or alter the normal settlement sequences of PP and cortical plate neurons.

Interaction of development and genetically targeted ablation in growth defects

If the only effect of genetically targeted ablation is permanent elimination of principal PP neurons, then pallial growth defects at P4 should be negligible because principal PP neurons normally account for only 1–2% of neocortical neurons at that age. Instead, the pattern of substantial, progressive reduction of growth in the ablated pallium indicates that the initial defect introduced by the specific killing of GPT cells is amplified by subsequent, faulty cellular interactions. Large-scale biological processes such as assembly of mammalian neocortex are obviously the developmental product of many concerted factors (Waddington, 1956; Debat and David, 2001). We use a composite *ablation* × *age* interaction in a robust, two-factor statistical model to represent their cumulative effect. However, a stereotyped sequence of faulty, interrelated cellular interactions, where each step contributes to the composite interaction, is also beginning to emerge. The natural occurrence of both the composite interaction and the sequence of its component cellular interactions is best observed during the *in situ* development of whole brain, since many of the component cellular interactions may be unavailable or inoperative in more restricted cell and tissue models.

As outlined above, specific killing of GPT cells produces only a few immediate changes, which occur mainly in pallial VZ. Excess dying GPT cells are temporarily stranded there, and their radial fibres are destroyed. These abnormal circumstances down-size and decelerate horizontal and vertical pallial growth within somatic and neuropil tissue compartments. Of greater importance, they also initiate a maturational delay for the settlement of principal PP neurons and introduce a morphogenetic discontinuity into the radial fibre network. Their destructive impact persists in the statistical model as the *ablation* main effect, which subtracts across age groups from constructive development normally represented by the *age* main effect.

The *ablation* main effect triggers subsequent defects of inductive, morphogenic and tropic cellular interactions (Edelman, 1988), which join the composite *ablation* × *age* interaction that increasingly subtracts between age groups from the *age* main effect. The earliest fault in the sequence is the distortion of a close-proximity, inductive interaction between dying GPT cells and non-GPT precursors in the VZ, which accelerates and prolongs precursor differentiation toward an intermediate progenitor, replacement GPT neuroblasts. This compensatory recruitment is accompanied by faulty morphogenic interactions that reconstitute the VZ proliferative array and further disrupt the radial fibre network (Xie et al., 2002, 2009). Reduction of horizontal and vertical growth arises from the restriction of the replacement VZ template, and the constriction of its physical translation into neocortex, as mediated by replacement PP neurons. The onset of these faults, and the *ablation* main effect, coincide with and are reflected by the early E12–E13 growth deflection.

A faulty morphogenic interaction next takes place, most likely between the degenerated radial fibre network and the delayed replacement GPT neurons, which then fail to emit long projection axons (Xie et al., 2009). These pioneer axons normally guide neocortical penetration of long afferent, particularly thalamocortical, axons (Molnar and Blakemore, 1995; Molnar et al., 1998; Hevner et al., 2002; Jacobs et al., 2007). In their absence, thalamocortical projections, most notably 'specific' thalamic relay connections for sensory systems, do not penetrate neocortical targets in an orderly fashion to elaborate characteristic terminal fields, usually initiated in immature neocortex (Auladell et al., 2000;

© 2010 The Author(s) This is an Open Access article distributed under the terms of the Creative Commons Attribution Non-Commercial Licence (http://creativecommons.org/licenses/by-nc/2.5/) which permits unrestricted non-commercial use, distribution and reproduction in any medium, provided the original work is properly cited.

Lopez-Bendito and Molnar, 2003). The onset of this defect coincides with and is reflected by the late E15–E16 growth deflection. The defect also extends to include associational and commissural corticocortical projections. Reduction of horizontal and vertical growth arises from the decreased frequency of axons in the neuropil tissue compartment and fibre tracts.

A faulty trophic interaction then occurs between the impoverished terminal fields of long axonal projections and neurons in mature neocortex, which curtail the outgrowth and branching of their dendrites and local axonal collaterals (Adams et al., 1997; Xie et al., 2009). Reduction of horizontal and vertical growth arises from the decreased frequency of neuronal processes in the neuropil tissue compartment. A final faulty trophic interaction proceeds between the inadequate synaptic connectivity conveyed by axons (afferent projection and local fibers) and neocortical neurons, which accelerates the pace of neuronal apoptosis and reduces growth in the somatic and neuropil tissue compartments during the third phase of the ablation (Cowan et al., 1984; Xie et al., 2002, 2009). It is interesting to note that this phase is accompanied by gross neuronal degeneration in subcortical sites, such as claustrum, normally predominated by reciprocal connections with neocortex.

This is not a full and exhaustive account of all abnormal cellular interactions that can take place in the ablated pallium, where the normal pattern of gradual, smooth and linear physical growth is largely maintained but progressively decelerated. In normal forebrain, such extensive, sequential interactions may buffer, regulate and synchronize development. In ablated forebrain, sequential cellular interactions underlie a constructive compensation that sustains pallial development, but sets in motion destructive consequences that limit its long-term success. In any event, the pathogenic amplification achieved by composite interaction shows that even modest delays of 24–48 h in the settlement of principal PP neurons can lead to many, if not all, of the same devastating structural defects claimed to be due to their selective, permanent elimination (Ghosh and Shatz, 1993).

Persistence of growth defects after genetically targeted ablation

Specifically killed GPT cells are clearly the nexus and intervening variable between experimental conditions (genotype, ganciclovir treatment and age at ganciclovir treatment) that cause genetically targeted ablation and its long-term phenotypic expression (Xie et al., 2002, 2009). We delineate a previously uncharted, immediate dose–response relationship between the ablation conditions and killed GPT neurons. Contingent on this outcome, a subsequent dose–response relationship unfolds between killed GPT neurons and persistent pallial growth defects. Both dose–response relationships are important demonstrations of the specificity of the genetically targeted ablation. However, the second relationship is technically constrained in at least three respects.

First, values for the independent variable, killed GPT neurons, are derived as a constant for each ablation group, not measured for each case within a group (although such observations prove to be feasible, and consistent with derived predicted values). In view of this limitation, all between-case, within-group variance of dependent variables is currently included in statistical error terms. This conservative solution underestimates the variance that should properly be attributed to killed GPT neurons. It also precludes multiple regression and factor analyses.

Secondly, the trigger episodes for the killing of GPT neurons are superimposed on normal morphogenetic processes, which require time to marshal the combination of constructive and destructive recovery mechanisms that lead to continued development and persistent, progressive growth defects. Extension of the post-ablation survival period allows the amplification of growth defects through sequential developmental interactions, but their increasing complexity tends to dilute the dose–response relationship between killed GPT neurons and growth defects. The step-like, stochastic clustering of outcomes for ablation groups with different levels of killed GPT cells suggests that some faulty cellular interactions do not contribute significantly to growth defects unless a minimum level of prior damage is attained (e.g. a threshold effect), while some faulty cellular interactions fail completely if a minimum level of prior damage is surpassed (e.g. a ceiling effect). Thus it is reasonable to propose that the 'severe ablation' cluster represents the full expression of the true ablation phenotype, while the 'mild ablation' cluster represents an intermediate version of the same ablation phenotype.

Thirdly, the genetically targeted ablation used in our longitudinal studies is actually a serial lesion of GPT cells related to each ganciclovir treatment, which further contributes to the clustered outcomes of different ablation groups (Finger et al., 1973). The sequence and timing of episodic killing of GPT neurons recruit distinct levels of defective interactions. GPT intermediate progenitors have a short cell cycle of approx. 10 h and generate six to seven cohorts of GPT neurons over a period of approx. 72 h (Xie et al., 2009). Killing of two or more consecutive, early cohorts of GPT neurons (36–81% losses of original complement), with minimum delays of 24 h for settlement of replacements, yields the catastrophic outcome of groups in the severe ablation cluster. In contrast, killing of a single early cohort of GPT neurons (18% loss) or two non-consecutive cohorts of GPT neurons (41% loss), with a minimum delay of 12 h for settlement of replacements, yields the survivable outcome of groups in the mild ablation cluster. Groups in the severe ablation cluster have impaired pioneer axons and afferent projections, which appear to be largely intact in groups in the mild ablation cluster. This difference suggests that cellular interactions underlying the outgrowth of sufficient pioneer axons for afferent guidance can tolerate short, but not long,

© 2010 The Author(s) This is an Open Access article distributed under the terms of the Creative Commons Attribution Non-Commercial Licence (http://creativecommons.org/licenses/by-nc/2.5/) which permits unrestricted non-commercial use, distribution and reproduction in any medium, provided the original work is properly cited.

delays of settlement of replacement GPT neurons, which constitute the permissive benefit actually obtained from the plasticity of precursors in the ablated VZ. The killing of two consecutive, late cohorts of GPT neurons on E13 (9% loss) leads to a mild ablation outcome because cellular interactions underlying the outgrowth of sufficient pioneer axons occur mostly before the cells are attacked.

We focus on the unscarred pallium of ablated mice because it retains sufficient structural integrity to preserve at least some functional role in neural processing and transmission. Yet, the pallium of severely ablated mice often has a second structural component composed of scar tissue. As shown previously (Xie et al., 2009) and now in extensive maps of the ablated neocortical surface, these scars arise as a product of non-specific bystander killing related to the early, avascular arrangement of a limited site marking the pallial boundaries of distribution for the anterior and middle cerebral arteries (Marin-Padilla, 1985). Scars, when present, do not alter the conclusions of the present study, since measurements based on total pallium (scarred plus unscarred tissue) and unscarred pallium yield consistent and comparable results. However, scars exhibit a low level of growth distinct from adjacent unscarred tissue. They fill a benign but non-essential gap in the development of ablated pallium until the late advent of hydrocephalus, after which the cellular fabric of both scarred and unscarred tissue is so compromised as to be unable to resist extreme thinning and ultimately fatal disruption (Xie et al., 2002).

Taken together, the new evidence shows that genetically targeted ablations of the principal PP neurons can cost up to half of the growth potential of the dorsal pallium in mice, a species with modest neocortical evolution. It is certain that such losses produce significant functional impairments consistent with the principle of mass action and the high degree of cytoarchitectural organization normally achieved in neocortex (Lashley, 1929; Jones, 1988). The apparent absence of neurological seizures is not surprising due to the global distribution, symmetric localization and insular nature of impoverished synaptic connectivity in the ablated neocortical phenotype (Cepeda et al., 2010). Because of the extensive evolutionary elaboration of neocortex, a structural loss in humans comparable with the severe ablation phenotype is likely to result in gross microtelencephaly, with marginal chances for fetal survival to birth (Jones, 1997; Striedter, 2005). However, structural loss in humans comparable with the mild ablation intermediate phenotype is more likely to result in survival. If asymmetrically biased to locations in one hemisphere, such mild forms of damage could distort the radial fibre network and contribute to the laminar alteration of cell density, neuronal disarray and pyramidal neuron misorientation found in clinical cases of (neo)cortical dysplasia associated with intractable pediatric epilepsy (Andre et al., 2007). It has not escaped our notice that such early defects are unpromising candidates for amelioration by stem cell replacement therapies, since even modest delays of settlement of well-sited, intrinsically generated replacements for principal PP neurons, derived from the same cell lineage as the original killed cells, lead to faulty cellular interactions and progressive growth defects in a comparable neocortical phenotype now characterized after genetically targeted ablation.

ACKNOWLEDGEMENTS

We thank Dr Anthony Campagnoni for the transgenic mice used in this work. We also thank Celia Campagnoni, Vance Handley, Yan Hong-Hu, Vilma Schonnman and Kathy Kampf for technical support. We acknowledge Dr Joaquin Fuster, Dr Richard Sutton, Dr Harry Vinters and Dr James Waschek for advice on the manuscript.

FUNDING

This work was supported by the National Institutes of Health [grant numbers NS33091 and NS23022].

REFERENCES

Adams NC, Lozsadi DA, Guillery RW (1997) Complexities in the thalamocortical and corticothalamic pathways. Eur J Neurosci 9:204–209.

Allendoerfer KL, Shatz CJ (1994) The subplate, a transient neocortical structure: its role in the development of connections between thalamus and cortex. Annu Rev Neurosci 17:185–218.

Andre VM, Wu N, Yamazaki I, Nguyen ST, Fisher R, Vinters H, Mathern G, Levine M, Cepeda C (2007) Cytomegalic interneurons: a new abnormal cell type in severe cortical dysplasia. J Neuropathol Exp Neurol 66:481–504.

Auladell C, Perez-Sust P, Super H, Soriano E (2000) The early development of thalamocortical and corticothalamic projections in the mouse. Anat Embryol (Berlin) 201:169–179.

Bayer SA, Altman J (1990) Development of layer I and the subplate in the rat neocortex. Exp Neurol 107:48–62.

Bayer SA, Altman J (1991) Neocortical Development, Raven Press, New York.

Cepeda C, Andre V, Vinters H, Fisher R, Levine M, Mathern G (2010) Epileptogenesis and cortical dysplasia. In Atlas of Epilepsies (Panayiotopoulus C, ed.), Springer, London.

Chenn A, McConnell SK (1995) Cleavage orientation and the asymmetric inheritance of Notch 1 immunoreactivity in mammalian neurogenesis. Cell 82:631–641.

Cowan WM, Fawcett JW, O'Leary DD, Stanfield B (1984) Regressive events in neurogenesis. Science 225:1258–1265.

Debat V, David P (2001) Mapping phenotypes: canalization, plasticity and developmental stability. Trends Ecol Evol 16:555–561.

Del Rio JA, Heimrich B, Borrell V, Forster E, Drakew A, Alcantara S, Nakajima K, Miyata T, Ogawa M, Mikoshiba K, Derer P, Frotscher M, Soriano E (1997) A role for Cajal–Retzius cells and reelin in the development of hippocampal connections. Nature 385:70–74.

D'Herde K, Mussche S, Roberg K (2003) Morphological changes in dying cells. In Cell Proliferation and Apoptosis (Hughes D, Mehmet H, eds.), pp. 201–232, BIOS Scientific Publishers, Oxford.

Edelman GM (1988) Topobiology, Basic Books, New York.

Ferguson GA (1971) Statistical Analysis in Psychology and Education, McGraw-Hill, New York.

Finger S, Walbran B, Stein DG (1973) Brain damage and behavioral recovery: serial lesion phenomena. Brain Res 63:1–18.

Ghosh A, Shatz CJ (1993) A role for subplate neurons in the patterning of connections from thalamus to neocortex. Development 117:1031–1047.

Guillery, RW (2002) On counting and counting errors. J Comp Neurol 447:1–7.

Hasling TA, Gierdalski M, Jablonska B, Juliano SL (2003) A radicalization factor in normal cortical plate restores disorganized radial glia and disrupted migration in a model of cortical dysplasia. Eur J Neurosci 17:467–480.

© 2010 The Author(s) This is an Open Access article distributed under the terms of the Creative Commons Attribution Non-Commercial Licence (http://creativecommons.org/licenses/by-nc/2.5/) which permits unrestricted non-commercial use, distribution and reproduction in any medium, provided the original work is properly cited.

Hevner RF, Miyashita-Lin E, Rubenstein JL (2002) Cortical and thalamic axon pathfinding defects in *Tbr1*, *Gbx2*, and *Pax6* mutant mice: evidence that cortical and thalamic axons interact and guide each other. J Comp Neurol 447:8–17.

Jacobs E, Campagnoni C, Kampf K, Reyes SD, Kalra V, Handley V, Xie R, Hong-Hu Y, Spreur V, Fisher R, Campagnoni AT (2007) Visualization of corticofugal projections during early cortical development in a τ-GFP-transgenic mouse. Eur J Neurosci 25:17–30.

Jacobs E, Kampf K, Macklin W, Reyes S, Campagnoni C, Givogri I, Handley V, Spreur V, Fisher R, Campagnoni AT (2009) Targeted overexpression of a golli-myelin basic protein isoform to oligodendrocytes results in aberrant oligodendrocyte maturation and myelination. ASN Neuro 1(4):art:e0017. doi:10.1042/AN20090029.

Jacobson, M (1970) Developmental Neurobiology, Holt, Rinehart and Winston, New York.

Jones E (1988) History of cortical cytology. In Cerebral Cortex. Vol. 1. Cellular Components of the Cerebral Cortex (Peters A, Jones E, eds.), Plenum Press, New York.

Jones KL (1997) Smith's Recognizable Patterns of Human Malformation, W.B. Saunders, Philadelphia, PA.

Kaufman MH (1992) The Atlas of Mouse Development, Academic Press, London.

Landry CF, Pribyl TM, Ellison JA, Givogri MI, Kampf K, Campagnoni CW, Campagnoni AT (1998) Embryonic expression of the MBP gene: identification of a promoter region that targets transgene expression to pioneer neurons. J Neurosci 18:7315–7327.

Lashley KS (1929) Brain Mechanisms and Intelligence, University of Chicago Press, Chicago, IL.

Lopez-Bendito G, Molnar Z (2003) Thalamocortical development: how are we going to get there? Nat Rev Neurosci 4:276–289.

Luskin MB, Shatz CJ (1985) Studies of the earliest generated cells of the cat's visual cortex: cogeneration of subplate and marginal zones. J Neurosci 5:1062–1075.

Marin-Padilla M (1971) Early prenatal ontogenesis of the cerebral cortex (neocortex) of the cat (*Felis domestica*). A Golgi study. I. The primordial neocortical organization. Z Anat Entwickl-Gesch 134:117–145.

Marin-Padilla M (1985) Early vascularization of the embryonic cerebral cortex: Golgi and electron microscopic studies. J Comp Neurol 241:237–249.

Marin-Padilla M (1998) Cajal–Retzius cells and the development of the neocortex. Trends Neurosci 21:64–71.

McConnell SK, Ghosh A, Shatz CJ (1994) Subplate pioneers and the formation of descending connections from cerebral cortex. J Neurosci 14:1892–1907.

Misson JP, Edwards MA, Yamamoto M, Caviness VS (1988) Identification of radial glial cells within the developing murine central nervous system: studies based upon a new immunohistochemical marker. Dev Brain Res 44:95–108.

Molnar Z, Blakemore C (1995) How do thalamic axons find their way to the cortex? Trends Neurosci 18:389–397.

Molnar Z, Adams R, Blakemore C (1998) Mechanisms underlying the early establishment of thalamocortical connections in the rat. J Neurosci 18:5723–5745.

Molyneaux BJ, Arlotta P, Menezes JRL, Macklis JD (2007) Neuronal subtype specification in the cerebral cortex. Nature Rev Neurosci 8:427–437.

Moolten FL (1986) Tumour chemosensitivity conferred by inserted herpes thymidine kinase genes: paradigm for a prospective cancer control strategy. Cancer Res 46:5276–5281.

Noctor SC, Flint AC, Weissman TA, Dammerman RS, Kriegstein AR (2001) Neurons derived from radial glial cells establish radial units in neocortex. Nature 409:714–720.

Ogawa M, Miyata T, Nakajima K, Yagyu K, Seike M, Ikenaka K, Yamamoto H, Mikoshiba K (1995) The reeler gene-associated antigen on Cajal–Retzius neurons is a crucial molecule for laminar organization of cortical neurons. Neuron 14:899–912.

Osheroff H, Hatten ME (2009) Gene expression profiling of preplate neurons destined for the subplate: genes involved in transcription, axon extension, neurotransmitter regulation, steroid hormone signaling, and neuronal survival. Cerebral Cortex 19(1):il26–il34.

Pontious A, Kowealczyk T, Englund C, Hevner RF (2008) Role of intermediate progenitor cells in cerebral cortex development. Dev Neurosci 30:24–32.

Price DJ, Willshaw DJ (2000) Mechanisms of Cortical Development, Oxford University Press, Oxford.

Rakic P (2005) Less is more: progenitor death and cortical size. Nat Neurosci 8:981–982.

Sarnat HB, Flores-Sarnat L (2002) Role of Cajal–Retziuz and subplate neurons in cerebral cortical development. Semin Pediatr Neurol 9:302–308.

Smart IHM (1973) Proliferative characteristics of the ependymal layer during the early development of the mouse neocortex: a pilot study based on recording the number, location and plane of cleavage of mitotic figures. J Anat 116:67–91.

Striedter GF (2005) Principles of Brain Evolution, Sinauer Associates, Sunderland, MA.

Super H, Uylings HB (2001) The early differentiation of the neocortex: a hypothesis on neocortical evolution. Cerebral Cortex 11:1101–1109.

Super H, Soriano E, Uylings HB (1998) The functions of the preplate in development and evolution of the neocortex and hippocampus. Brain Res Rev 27:40–64.

Valverde F (1998) Golgi Atlas of the Postnatal Mouse Brain, Springer, Wien.

Valverde F, De Carlos JA, Lopez-Mascaraque L (1995) Time of origin and early fate of preplate cells in the cerebral cortex of the rat. Cerebral Cortex 5:483–493.

Van Cruchten S, Van den Broeck W (2002) Morphological and biochemical aspects of apoptosis, oncosis and necrosis. Anatom Histol Embryol 31:214–223.

Waddington CH (1956) Principles of Embryology, George Allen and Unwin, London.

Walsh C, Cepko CL (1993) Clonal dispersion in proliferative layers of developing cerebral cortex. Nature 362:632–635.

Xie Y, Skinner E, Landry C, Handley V, Schonmann V, Jacobs E, Fisher R, Campagnoni AT (2002) Influence of the embryonic preplate on the organization of the cerebral cortex: a targeted ablation model. J Neurosci 22:8981–8991.

Xie Y, Jacobs E, Fisher RS (2009) Targeted ablation and reorganization of the principal preplate neurons and their neuroblasts identified by golli promoter transgene expression in neocortex of mice. ASN Neuro 1(4):art:00018. doi:10.1042/AN20090038.

Received 28 June 2010/28 July 2010; accepted 2 August 2010

Published as Immediate Publication 7 September 2010, doi 10.1042/AN20100022

© **2010 The Author(s)** This is an Open Access article distributed under the terms of the Creative Commons Attribution Non-Commercial Licence (http://creativecommons.org/licenses/by-nc/2.5/) which permits unrestricted non-commercial use, distribution and reproduction in any medium, provided the original work is properly cited.